Palaeogeography, Palaeoclimatology, Palaeoecology 586 (2022) 110759

Contents lists available at ScienceDirect

Palaeogeography, Palaeoclimatology, Palaeoecology

journal homepage: www.elsevier.com/locate/palaeo

Climate-driven drainage reorganization of small mountainous rivers in Taiwan (East Asia) since the last glaciation: The Zhuoshui River example

Shuo Zhang [a,b], Xing Jian [b,*], James T. Liu [c], Ping Wang [d,e], Yuan-Pin Chang [c], Wei Zhang [b]

[a] Collaborative Innovation Center of South China Sea Studies, Nanjing University, Nanjing, Jiangsu Province, PR China
[b] State Key Laboratory of Marine Environmental Science, College of Ocean and Earth Sciences, Xiamen University, Xiamen, Fujian Province, PR China
[c] Department of Oceanography, National Sun Yat-sen University, Kaohsiung, Taiwan
[d] School of Geography, Nanjing Normal University, Nanjing, Jiangsu Province, PR China
[e] Jiangsu Center for Collaborative Innovation in Geographical Information Resource Development and Application, Nanjing, Jiangsu Province, PR China

ARTICLE INFO

Editor: Paul Hesse

Keywords:
Provenance analysis
Climate change
Source-to-sink
Late Quaternary
East Asia
Clay minerals

ABSTRACT

As an important component in East Asia sediment source-to-sink systems, small mountainous rivers in Taiwan deliver disproportionately large amounts of sediments to oceans. Although the modern fluvial sediment transport processes, discharge fluxes and sediment compositions have been well investigated, the drainage evolution of these mountainous rivers remains understudied and sediment fluxes are expected to vary greatly in glacial-interglacial cycles due to the tremendous climatic fluctuations. To define how the drainage of Taiwan mountainous rivers has evolved since the last glaciation, we target a sediment core (98 m in length) from the Zhuoshui River delta, western Taiwan and conduct sediment petrography, heavy mineral analysis, detrital zircon U—Pb geochronology and clay mineralogy to investigate provenance variations and river basin evolution since 60 ka. Sediments of the last glaciation show comparatively high illite crystallinity index values, low metasedimentary lithic fragment and stable heavy mineral contents and similar detrital zircon U—Pb ages with downstream signatures, indicating prominent sediment contributions from the Coastal Plain and Western Foothills regions (elevation <1 km) during the glaciation. However, characteristics of the deglacial and Holocene sediments indicate high contributions from the higher Hsueshan Range and Central Range regions (elevation >1 km). We suggest that headward extension and drainage capture since the deglaciation, which was most likely due to the increasing monsoon rainfall, account for the provenance variations in the discharged sediments. This implies a climate-driven drainage reorganization of the small mountainous rivers in Taiwan since the last glaciation. Our findings highlight the previously-overlooked, variable provenance information from Taiwan in glacial-interglacial cycles, and the dynamic source signatures are important to East Asia sediment source-to-sink studies.

1. Introduction

Continental margins are an important sink for terrestrial sediments. More than 90% terrigenous clastic materials are deposited on continental shelves (Thomas et al., 2004; Deng et al., 2006; Kao et al., 2008), although continental shelves account for only ca.7.5% of the global oceans (Postma, 1988). Because of the unique tectonic settings, monsoon climate, diverse landforms and bedrock lithology in the east and southeast Asia and the huge sediment discharge (ca. 70% on the global scale) from the exoreic rivers therein, the source-to-sink process of the sediments deposited on the east and southeast Asia continental margins has attracted considerable attention for decades (Milliman et al., 1985a, 1985b; Milliman and Syvitski, 1992; Yang et al., 1992; Ludwig and Probst, 1998; Sun et al., 2000; Meybeck et al., 2003; Walling and Fang, 2003; Yang and Liu, 2007; Kao et al., 2008, Kao et al., 2011; Xu et al., 2009; Li et al., 2012a, 2017, 2018; Shi et al., 2019). There is no doubt that the large rivers, such as the Yangtze River, Pearl River and Mekong River, supply large amounts of sediments to the east and southeast Asia continental margins (Milliman and Meade, 1983, Fig. 1a). Small mountainous rivers, particularly those draining tectonically active, subtropical-tropical Asian regions, also play a significant role in sediment supply-transport processes for those margins.

* Corresponding author at: State Key Laboratory of Marine Environmental Science, College of Ocean and Earth Sciences, Xiamen University, Xiamen, Fujian Province 361102, PR China.
E-mail addresses: shzhang@smail.nju.edu.cn (S. Zhang), xjian@xmu.edu.cn (X. Jian), james@mail.nsysu.e.tw (J.T. Liu), tigerwp@njnu.edu.cn (P. Wang), yuanpin.chang@mail.nsyu.edu.tw (Y.-P. Chang), zhangwei6387@163.com (W. Zhang).

https://doi.org/10.1016/j.palaeo.2021.110759
Received 29 April 2021; Received in revised form 27 October 2021; Accepted 8 November 2021
Available online 15 November 2021

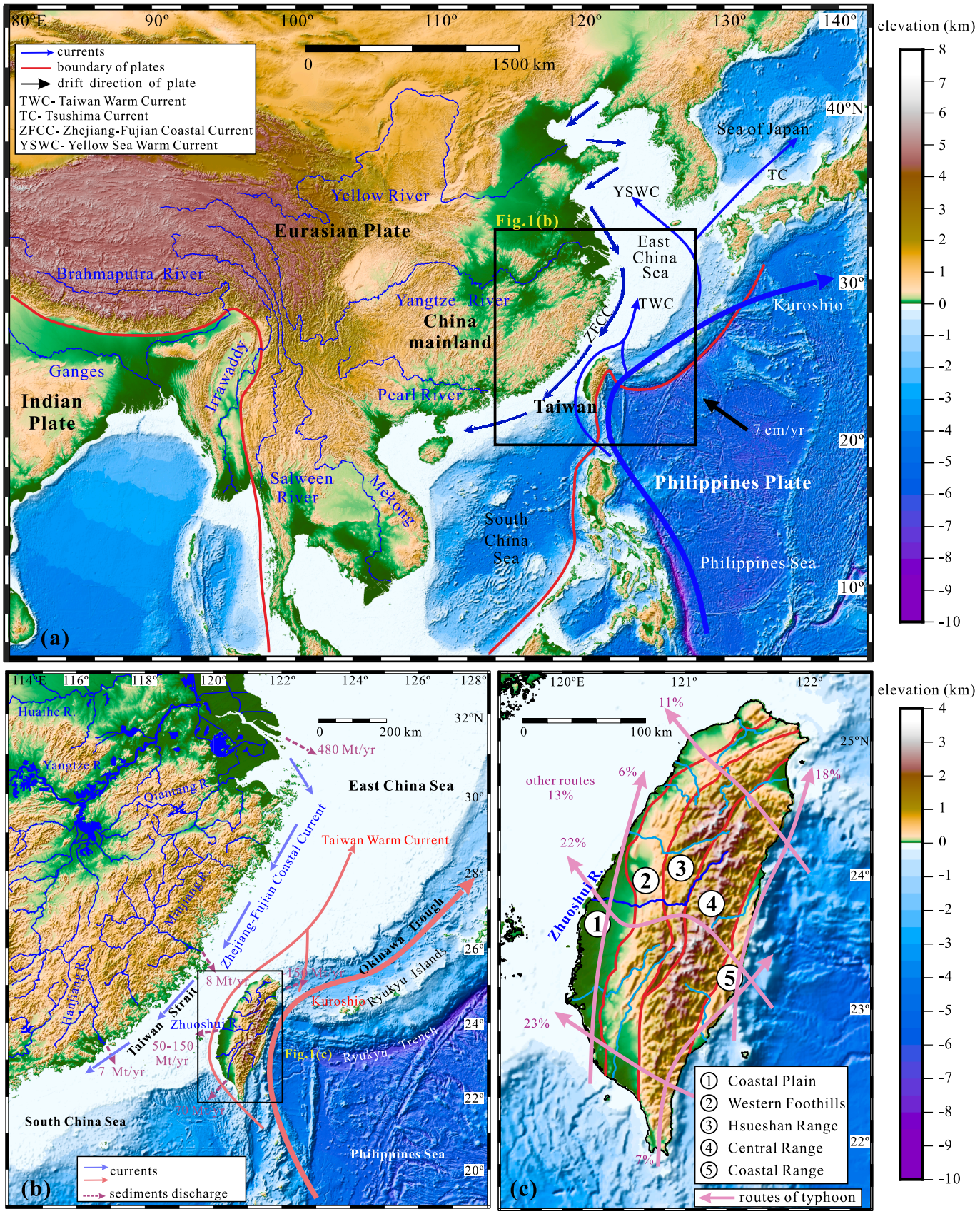

Fig. 1. (a) Overview map of major rivers and currents in East Asia. The ocean current routes are from Han et al. (2012), the plate movement rates are from Seno et al. (1993). (b) Location of major rivers, currents and annual sediments flux of rivers in southeast China (Milliman and Meade, 1983; Liu et al., 2008a). (c) The tectonic framework of Taiwan and routes of typhoons (Chai, 1972; Liu et al., 2013). The geographic maps generated by Generic Mapping Tools (Wessel et al., 2019).

Small mountainous rivers, are defined as rivers with original elevation higher than 1000 m and drainage area less than 10,000 km^2, such as rivers in Taiwan and Luzon Island, East Asia (Fig. 1b, Milliman and Syvitski, 1992). Although the drainage areas cover less than 10% of the global terrestrial regions that drains to the ocean, the small mountainous rivers on the Earth contribute about 15% of water, 45% of clastic sediments, 30% of dissolved solids and nearly half of particulate organic carbon to the global ocean (Milliman and Syvitski, 1992; Lyons et al., 2002; Leithold et al., 2006; Hilton et al., 2008; Milliman and Farnsworth, 2011). Therefore, small mountainous rivers serve as key carriers of sediments in the source-to-sink processes and provide crucial links between lands and oceans. Furthermore, small mountainous rivers are quite sensitive to extreme tectonic or climatic events (Chikita et al., 2002; Kao et al., 2005b; Xu et al., 2009; Tarazón et al., 2010), and thus provide important test grounds for tracking critical geological processes on the Earth's surface.

Given the remarkable climatic fluctuation between glacial and interglacial periods, sediment source-to-sink systems involving small mountainous rivers may vary obviously. Previous case studies on global small mountainous rivers have proposed several different driving mechanisms for glacial and interglacial variations in sediment supply, transport and deposition and in sediment compositions. These mainly include (1) varied erosion dynamics, e.g., shifting from glacier carving to landslide (Jiao et al., 2018); (2) different denudation rates, controlled by precipitation glacier ranges, especially in mid and high latitudes (Mariotti et al., 2021); (3) variable residence time of sediments in source-to-sink systems due to changes in physical erosion rates and patterns (Zhao et al., 2017); (4) environmental changes in drainage basins and in depositional areas (Yang et al., 2017). Although none of these driving mechanisms account for all the variations in global small mountainous rivers-related sediment source-to-sink systems in glacial-interglacial cycles, more and more studies have been aware of the remarkable variations and their influences in controlling the evolution of the Earth's surface.

Taiwan is located at the boundary between the Eurasian and Philippines Plates. Taiwan Island is characterized by tectonically active backgrounds and frequent earthquakes. Subtropical monsoon climate currently prevails and tropical cyclones frequently influence Taiwan, resulting in large amount of rainfall in summer and fall (Huang et al., 1997; Liu et al., 2001, 2013; Kao et al., 2008). Additionally, Taiwan is one of the densest river-covered regions in Asia. Specially, the total length of rivers in Taiwan extends more than 42,000 km and have average drainage density of 1.17 m/km^2 (Li et al., 2012a), with incision rates of ~6.4 to ~16 mm/yr (Dadson et al., 2003). As a result, Taiwanese rivers annually supply approximately 180–380 Mt. sediments to adjacent oceans, such as the Taiwan Strait, Okinawa Trough, East China Sea, South China Sea (Fig. 1b, Kao et al., 2006a, 2006b; Liu et al., 2008b). Therefore, Taiwan is regarded as an ideal site to study sediment transport and discharge by small mountainous rivers (Dadson et al., 2004; Kao et al., 2005a).

Although the small mountainous rivers in Taiwan currently retain high sediment flux under such tectonic and climatic conditions (Milliman and Syvitski, 1992), these rivers might have comparatively low sediment discharges during glaciations. For example, sediment records in the estuary area of the Zhuoshui River indicate that during the last glaciation, the depositional rate was low (Yang et al., 2017; Zhao et al., 2017). However, why the sediment outputs varied during the last glaciation remains poorly known. The climatic characteristics in Taiwan have changed significantly since the end of last glaciation, such as strengthening of the East Asian summer monsoon (Chen et al., 2017a, 2017b), westward moving and strengthening of the Kuroshio Current (Jian et al., 2000; Dou et al., 2015, 2016), melting of mountainous glaciers (Böse, 2004; Ono et al., 2005; Hebenstreit et al., 2006), more frequent typhoons (Chen et al., 2012; Wang et al., 2014), increasing of rainfall (Yang et al., 2011; Cheng et al., 2016; Clemens et al., 2018), as well as rapidly-rising sea level. Logically, the following processes can be potential reasons for the depositional rate increase from the last glaciation to the Holocene. 1) Mountainous glaciers retreated and the erosion rate in mountainous regions changed; 2) the increased precipitation led to more erosion and transport of sediment; 3) the fluctuation of sea level caused the change of transport and deposition processes and 4) extended drainage basin received more sediments discharge.

To define the mechanism of the depositional rate variation, we collected sediment samples from a drilled core (JRD-N) at the Zhuoshui River delta. Given the contrasting bedrock lithologies of the upstream and downstream regions in the Zhuoshui River catchment (Fig. 2a), framework grain petrography, heavy mineral analysis, detrital zircon U—Pb geochronology and clay mineral analysis were employed to conduct an integrated provenance analysis for both mud and sand samples. The objective of this study is 1) to evaluate compositional variations of the sediments discharged by the Zhuoshui River over millennial-scales, 2) to track sediment provenance and 3) to investigate controlling mechanisms for provenance variations since the last glaciation.

2. Background of Taiwan and the Zhuoshui River

The Taiwan Island is about 370 km long and 145 km wide, with NNE extending, and is situated at the boundary between the Eurasian and Philippines Plates (Huang et al., 1995, 2012, Fig. 1a). To the south of the island, the oceanic crust of South China Sea subducts beneath the Philippines Plate along the Manilla Trench, which leads to the formation of the Luzon Arc (Briais et al., 1993; Yang et al., 1996). To the east of the island, the Philippines Plate subducts northwestward along the Ryukyu Trench with a rate of 70 mm/yr (Seno et al., 1993, Fig. 1a). As a consequence of the Philippines Plate subduction, the North Luzon Arc has collided with Eurasian Plate at the Longitudinal Valley (located in eastern Taiwan), and the Taiwan Island began uplifting at 6.5 Ma (Chai, 1972; John et al., 1990; Huang et al., 1995, 1997; Malavieille et al., 2002; Li et al., 2007; Zhang et al., 2016). The Taiwan Island can be divided into five tectonic units, i.e., Coastal Plain, Western Foothills, Hsueshan Range, Central Range and Costal Range from west to east (Ho, 1986; Chen and Wang, 1995; Liu et al., 2001, Fig. 1c). Because of the tectonically active background, the Taiwan Island has been uplifted rapidly, with an exhumation rate of about 5–10 mm/yr (Dadson et al., 2003; Hsu et al., 2016). More than 2500 earthquakes with the Richter magnitude $\geq$4.0 occurred in Taiwan and the adjacent areas during 1950 to 2018 (data from National Earthquake Data Center, China).

Bedrock in Taiwan is dominated by Tertiary marine siliciclastic sedimentary and metasedimentary rocks, with subordinate Mesozoic strata (Fig. 2a). These sedimentary strata distribute narrowly along the tectonic units. The Coastal Range is dominated by Miocene to Quaternary strata. The Central Range consists of Mesozoic basement (Tananao Complex), East Taiwan Ophiolite with a formation age of ~15 Ma (Lin et al., 2019), and Eocene to Miocene strata, and the basement metamorphosed during late Cenozoic (Chen et al., 2017a, 2017b). The Hsueshan Range is an Eocene to Early Oligocene slate formation. The Western Foothills is composed of sedimentary rocks with depositional ages from the late Oligocene to Pleistocene. The Coastal Plain is covered by Holocene deposits formed by fluvial erosion (Ho et al., 1964; Huang and Ting, 1979; Huang, 1986; Chen et al., 2019). Igneous rocks are sporadically exposed in Taiwan, which are dominated by volcanic rocks, i.e., volcanos in Datun and Keelung, andesite and quartz andesite in Coastal Range, and basalt in Penghu Islands (Ho et al., 1964; Li et al., 2012a).

The Zhuoshui River, as the longest river (186.4 km) in Taiwan, originates from the Central Range with the elevation over 3400 m, erodes the Hsueshan Range, Western Foothills and Coastal Plain from east to west, and finally flows into the Taiwan Strait (Fig. 1c). The drainage basin covers about 3155 km^2 (Milliman and Syvitski, 1992; Lee et al., 2016) and the bedrock therein is mainly composed of (meta) sedimentary rocks, including Eocene to Miocene slate and phyllite,

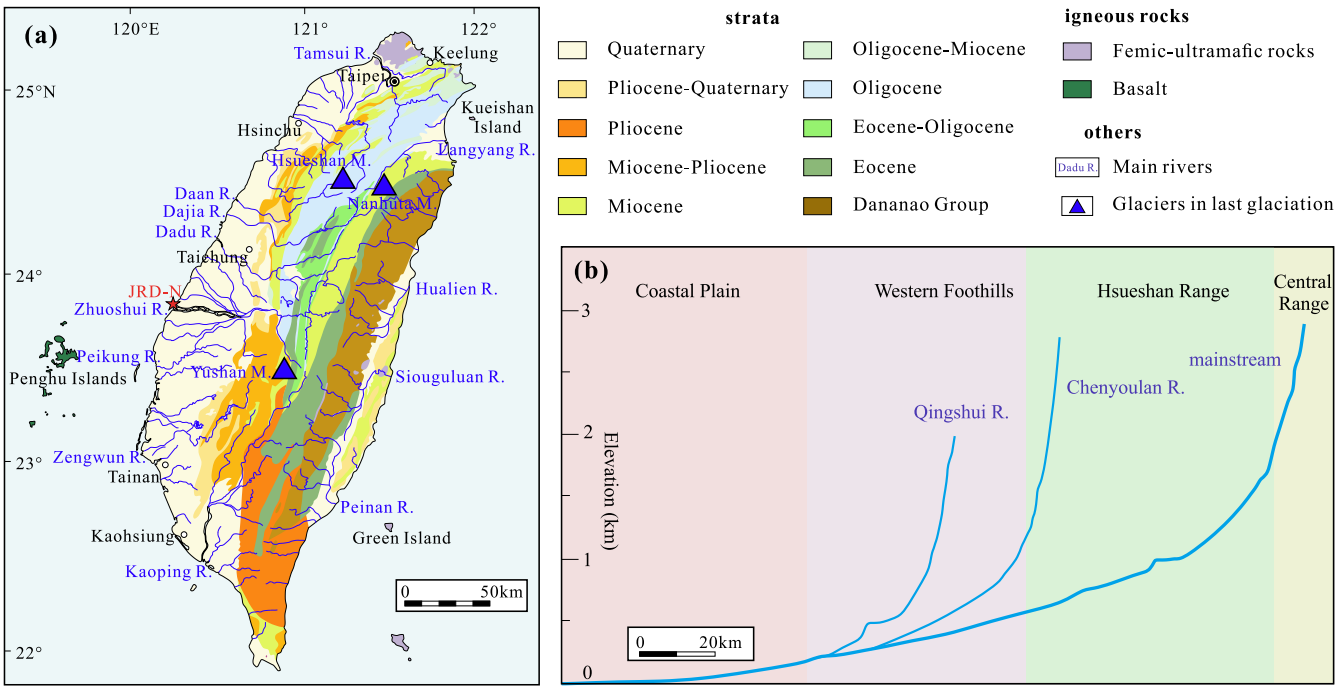

Fig. 2. (a) The geological map of Taiwan, the map followed Bureau of Geology and Minerals of Fujian Province, 1986, the location of glaciers followed Cui et al. (2002). (b) Topographic profile along the mainstream and two major tributaries (Deng et al., 2020).

Eocene to Pleistocene shale, sandstone and turbidite, and Holocene alluvial deposit (Huang et al., 2012; Zhao et al., 2017, Fig. 2a).

Rainfall is abundant in Taiwan, with an average annual precipitation of 2500 mm (Garzanti and Resentini, 2016). For this reason, the Zhuoshui River discharges about 54 Mt. sediments to the Taiwan Strait every year (Deng et al., 2019). Typhoons are frequent in Taiwan, 255 typhoons passed through Taiwan in 1949–2009, with an average of approximately 4 per year (Liu et al., 2013). The routes of typhoons were

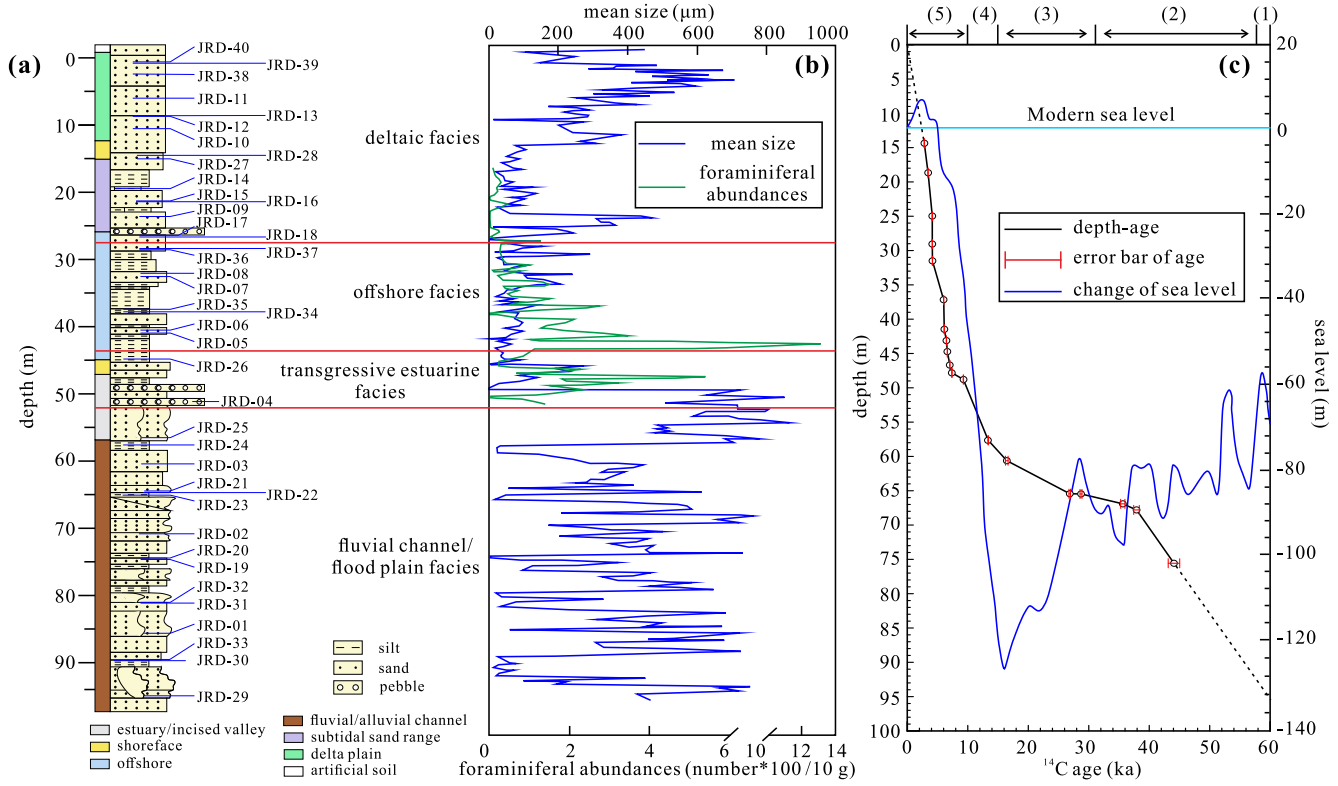

Fig. 3. (a) Down-core plots of the sedimentary and lithofacies for JRD-N. (b) The foraminiferal abundance and mean size for JRD-N. (c) The age model of core JRD-N and variation of sea level. The information of Core JRD-N followed Yang et al. (2017), the variation of sea level followed Bard et al. (1990). The partition of last glaciation followed Yao (1997): (1) early stadial stage: 75–48 ka; (2) interstadial stage: 48–32 ka; (3) LGM: 32–15 ka; (4) deglaciation:15–11.7 ka; (5) Holocene: 11.7–0 ka.

shown in Fig. 1c. During typhoon events, the small mountainous rivers can supply and discharge large amounts of sediments within a few days (Milliman et al., 2017). For example, the Zhuoshui River discharged 68 Mt. and 175 Mt. sediments to the ocean during the typhoon Herb in 1996 and the typhoon Toraji in 2001, respectively (Dadson et al., 2005). About 75% of rainfall concentrates in the period of May–October (Kao and Milliman, 2008), and suspended sediment concentrations of the Zhuoshui River in summer to autumn often reach levels of 40 g/L, which are ten times higher than those in dry seasons (Xu et al., 2009).

3. Samples and methods

3.1. Sample descriptions

A 98-m long sediment core (named as JRD-N, at 120°18.15′E, 23°54.17′N) was drilled on the upper tidal flat at an elevation of 7.94 m in the northern tidal basin of the Zhuoshui River mouth (Fig. 2a) in 2010. The lithofacies were previously described by Yang et al. (2017) and are also shown in Fig. 3(a, b). The accelerator mass spectrometer (AMS) in NSF-Arizona AMS Laboratory at University of Arizona was employed to obtain ^{14}C ages. Dating material included mollusk shells, plant matter, and peat (Yang et al., 2017). The age model was built as follows. First, the three oldest dating points were performed in linear regression and were calculated the root mean square error (RMSE). Then, the adjacent younger point was added and re-calculated the RMSE. The age point was employed in the age model only if the RMSE was equal to or less than previous number. Third, repeated the second process until the age model was completed (Fig. 3c). The ages of the analyzed samples were calculated by the linear interpolation method. Detailed age datasets and age model building procedures for the sediment core were also given by Yang et al. (2017).

Eight kinds of sedimentary facies of the sedimentary strata were recognized in the core JRD-N, including (1) fluvial channel, (2) floodplain, (3) estuary, (4) shoreface, (5) offshore, (6) sub-tidal sand ridge, (7) delta plain facies, and (8) perturbed soil (Yang et al., 2017). And were grouped into four units, i.e., fluvial channel/flood plain facies in 50–18 ka, transgressive estuarine facies in 18–8 ka, late transgressive to early offshore facies in 8–4.5 ka, and deltaic facies in 4.5–0 ka (Fig. 3a, Yang et al., 2017). The age-elevation model exhibits a turning point at ~13 ka, which indicates the deposition rate increased from less than 0.8 mm/yr to 2.5–4 mm/yr (Fig. 3c). Additionally, the foraminiferal biomass increased at this turning point (Fig. 3b).

3.2. Analytical methods

3.2.1. Sandy sediments

Sandy sediments were selected for framework grain petrography, heavy mineral analysis and detrital zircon U—Pb dating.

Twenty-two sand samples were selected for framework grain petrography analysis. The 0.063–0.5 mm fractions were separated, impregnated with araldite. The solidified samples were sliced into 0.03-mm thin sections. These thin sections were then analyzed by counting approximately 400 points under a polarizing microscope. Major framework grains, including quartz, plagioclase, K-feldspar, and various lithic fragments, were identified (Fig. S1 in Supporting Information S1), and identification of minerals and lithic fragments were based on characteristics described by Chang et al. (2010).

Twenty sand samples were selected for heavy mineral composition analysis. Heavy minerals were separated by heavy liquid tribromomethane (2.89 g/cm^3) from the fractions with grain size of 0.063–0.5 mm and subsequently impregnated on glass slides with Canada balsam. About 200 heavy mineral grains were identified and point-counted at suitable regular spacing under a polarizing microscope. The identification of heavy minerals was based on characteristics described by Mange and Maurer (1992). The separation and identification of heavy minerals were carried out in the Sedimentary Geology Laboratory, Xiamen University, following standard procedures described by Jian et al. (2020).

Two samples JRD-25 (deposition age = ~13 ka) and JRD-31 (DA = ~48 ka) were selected for detrital zircon U—Pb dating. Zircon grains were separated using heavy liquids and magnetic separation techniques, and then mounted in epoxy grain mounts along with the Plěovice zircon and NIST610 glass reference materials (Sláma et al., 2008). The zircon crystals were then examined with transmitted and reflected lights. The U—Pb isotopes were measured using an Agilient 7500a ICP-MS coupled to a GeoLas200M 193 nm ArF-excimer laser-ablation system at the LA-ICP-MS laboratory, Nanjing Normal University, China. The analyses were conducted with a 32 μm diameter beam with fluence of 15 J/cm^2 at 4 Hz. The typical ablation pit depth was 35–50 μm. Isotopic ratios were calculated with the GLITTER software package and were corrected for common-Pb by the approach described by Andersen (2002). Isoplot 3.0 (Ludwig, 2012) was used to determine the zircon U—Pb ages and to generate concordia plots. Following the conventional reporting of detrital zircon ages, the ages with poor precision (> ±10%), high discordance (> ±20%) were omitted from the probability density function, the kernel density estimation (KDE) plots (Vermeesch, 2012) and from interpretation. The $^{207}Pb/^{206}Pb$ ages and $^{206}Pb/^{238}U$ ages were adopted for grains older than 1000 Ma and for younger than 1000 Ma, respectively (Gehrels et al., 2006, 2008; Jian et al., 2019; Zhang et al., 2021).

3.2.2. Silty and mud sediments

Twenty-nine silty and mud sediment samples were selected for clay mineral composition analysis. The <2 μm fractions were first separated, based on conventional Stokes' settling velocity principles (after removing the carbonate and organic matter with 1 mol/L acetic acid and 10% hydrogen peroxide, respectively). Each sample was transferred to slide by wet smearing, air-dried and made as an oriented mount. These oriented mounts were then placed in a vacuum pressure box and were saturated with ethylene-glycol vapor for at least 48 h (Mei et al., 2021). A Rigaku Ultima IV X-ray diffractometer (XRD) at Xiamen University was used for total clay fraction (<2 μm) composition analysis. Each sample was continuously scanned under 40 kV, 30 mA, with wave length of 1.54, degree range of 4° to 30°, and step width of 0.02° conditions. Scanning speeds were 4°/min. The software Jade 6.0 was used in data analysis. Representative oriented mounts were also measured directly after air-drying treatment and after 2 h 500 °C heating treatment to identify smectite, illite, kaolinite and chlorite (Li et al., 2012a). The semi-quantitative estimation of clay minerals was based on XRD diagrams of ethylene-glycol treated mounts (Fig. S2), using the Biscaye (1965) method. Relative percentages of clay minerals were determined using ratios of integrated peak areas of (001) series of their basal reflections according to the XRD diagrams, and were weighted by empirically estimated factor. The detailed XRD peaks of (001) series include 17 Å (smectite), 10 Å (illite), 7 Å (kaolinite and chlorite). And the 3.57 Å/3.54 Å peak intensity ratios were used for calculating kaolinite and chlorite contents. We followed the calculation methods described by Mei et al. (2021). Illite crystallinity index was estimated as the full width at half maximum of the 10 Å (Holtzapffel, 1985; Liu et al., 2008b; Mei et al., 2021).

4. Results

4.1. Framework grain compositions

Framework grains of the analyzed sand sediments are mainly composed of lithic fragments, which account for more than 50% of the framework grains. The proportions of sedimentary lithic fragments (Ls) therein are the highest (24.5%–73.4%). Metamorphic lithic fragments (Lms) occupy the proportions of 12%–32.6% and are dominated by metasedimentary lithic fragments. Igneous lithic fragments (Lv) show low abundances, with the proportion of less 1%. The abundances of

quartz and feldspar are low, with the relative proportions of 2.2%–20.1% and 6.9%–41.5%, respectively (Fig. S3). Both K-feldspar and plagioclase in the Holocene samples show higher relative proportions than those in last glaciation samples. The ratios of Lms/Ls increase significantly for the deglacial and Holocene samples (with an average ratio of 0.56), compared to those for the last glaciation samples (with an average ratio of 0.19, Fig. 4e).

4.2. Heavy mineral compositions

The proportions of opaque minerals, transparent heavy minerals with high abundance are shown in Fig. S4. The ZTR index (the proportions of zircon, tourmaline and rutile in all the transparent heavy minerals) values are illustrated in Fig. 4 f. The opaque mineral proportions are relatively high, with a range of 41%–72% (mean 56%). Garnet is the most abundant transparent mineral, ranging from 0.8% to 24% (mean 11%). The abundances of tourmaline and zircon which represent stable components are relatively low, with range of 0–8% (mean 5%) and 0–16% (mean 2%), respectively. In addition, apatite, titanite and epidote are also present in the samples. The characteristics of the observed heavy minerals reflect low compositional maturity. The ZTR index values are quite low for the last glaciation samples (with an average value of 15.6), and are comparatively high for the Holocene samples (with an average value of 23.6, Fig. 4f).

4.3. Detrital zircon U—Pb ages

One hundred detrital zircon grains were analyzed for each sample and the results are shown in Table S1 in Supporting Information S2. The U/Th ratios (Fig. S5) indicate that most detrital zircons are of igneous origin. Seventy-six concordant ages were obtained for sample JRD-25 (Fig. S6a), ranging from 86.6 ± 1.5 Ma to 2663 ± 26 Ma. The age populations cluster into five major age groups: 85–260 Ma, 160–460 Ma, 560–1100 Ma, 1500–2100 Ma and 2200–2600 Ma, with two major age peaks at 108 Ma, 435 Ma and two secondary age peaks at 798 Ma and 1838 Ma (Fig. 5g). Eighty-four concordant ages were obtained for sample JRD-31 (Fig. S6b) and these ages ranges from 37.3 ± 0.7 Ma to 3102 ± 14 Ma. The age populations cluster into four major age groups: 100–300 Ma, 400–1000 Ma, 1000–1600 Ma, 1600–2700 Ma, with four major age peaks at 408 Ma, 775 Ma, 1851 Ma, 2500 Ma and several secondary age peaks (Fig. 5h).

4.4. Clay mineral compositions

The clay mineral compositions are shown in Fig. 4, and the detailed data are shown in Table S2. Illite exhibits high proportions in the samples (58%–94%), while the abundances of chlorite and kaolinite are comparatively low, with relative proportions of 4%–23% and 1%–13%, respectively. Smectite is scarce in most samples but the proportion of smectite in sample JRD-38 is 23%. Kaolinite exhibits less proportion in last glaciation samples (averaging 4%) than those in the Holocene samples (averaging 6%). The average abundance of illite in last glaciation samples is 80% and the Holocene samples retain an average illite abundance for 75%. The illite crystallinity index values vary significantly, with a range of 0.17°– 0.554°Δ2θ, and show obvious variations among different samples. The illite crystallinity index values of samples for the interstadial stage are relatively low, with an average 0.259°Δ2θ. The LGM samples exhibit an average value of 0.396°Δ2θ, and the Holocene samples have the illite crystallinity index values averaging in 0.305°Δ2θ.

5. Interpretation and discussion

5.1. Provenance of the analyzed core sediments from the Zhuoshui River delta

The modern Zhuoshui River, as a typical small mountainous river, is only 186 km long, with a steep slope (Fig. 2b). The modern sediments are considered to be poorly sorted by the river flow (Deng et al., 2016). Additionally, abundant sediments could be carried to the river mouth region by rapid erosion-transport-deposition processes which often occur due to extreme events (Dadson et al., 2004, 2005; Milliman et al., 2007). As a result, sediments experience weak chemical weathering due to short residence time (Dadson et al., 2005; Li et al., 2012a, 2016). The $^{234}U/^{238}U$-based comminution ages (indicating the timescale of sediments source-to-sink processes) for the Zhuoshui River sediments are estimated to be ~110 ka (Li et al., 2016). Therefore, the analyzed Zhuoshui River delta sediments probably cannot directly reflect the variations of chemical weathering intensity of bedrocks in Taiwan since the last glaciation (began at ~75 ka), although previous study suggested that the chemical weathering intensity of sediments in Zhuoshui River was slightly higher than that in the Holocene (Fig. 4d, Zhao et al., 2017). This means that the sediment compositions (including mineralogical and geochemical compositions) are insensitive to the climate changes and the chemical weathering alterations. Instead, the discharged sediments of Taiwan rivers were mainly controlled by parent-rock lithology (Garzanti and Resentini, 2016), and we suggest that the temporal composition variations of the core JRD-N are seemly caused by contribution changing of different source regions.

5.1.1. Provenance of sand

Both the framework grain and heavy mineral compositions of the

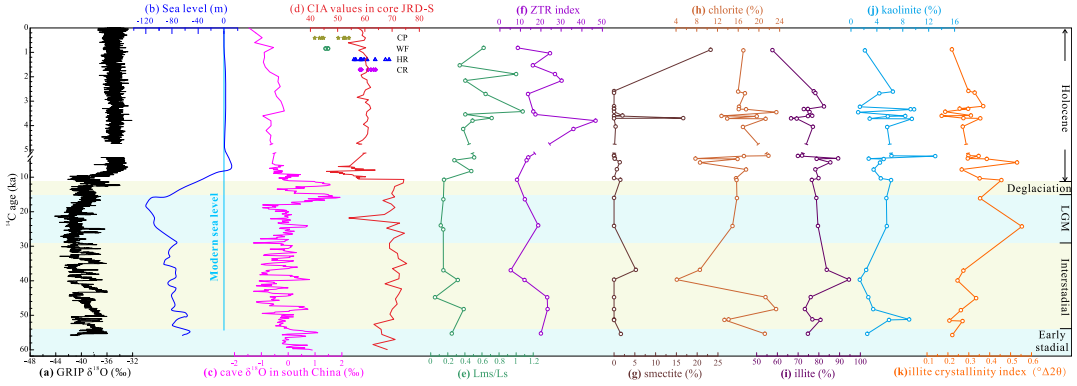

Fig. 4. (a) $\delta^{18}O$ of Greenland Ice Core Project (GRIP, Seierstad et al., 2014 and reference therein). (b) The change of sea level (Bard et al., 1990). (c) the cave $\delta^{18}O$ in south China (Cheng et al., 2016). (d) The comparation of CIA values in core JRD-N (Zhao et al., 2017) and source areas (Deng et al., 2019). Abbreviation: CP-coastal Plain, WF-Western Foothills, HR-Hsueshan Range, CR-Central Range. (e) The ratio of metamorphic lithic fragments/sedimentary lithic fragments in Core JRD-N. (f) The ZTR index in Core JRD-N. (g–j) The clay mineral contents in Core JRD-N. (k) Illite crystallinity index in Core JRD-N.

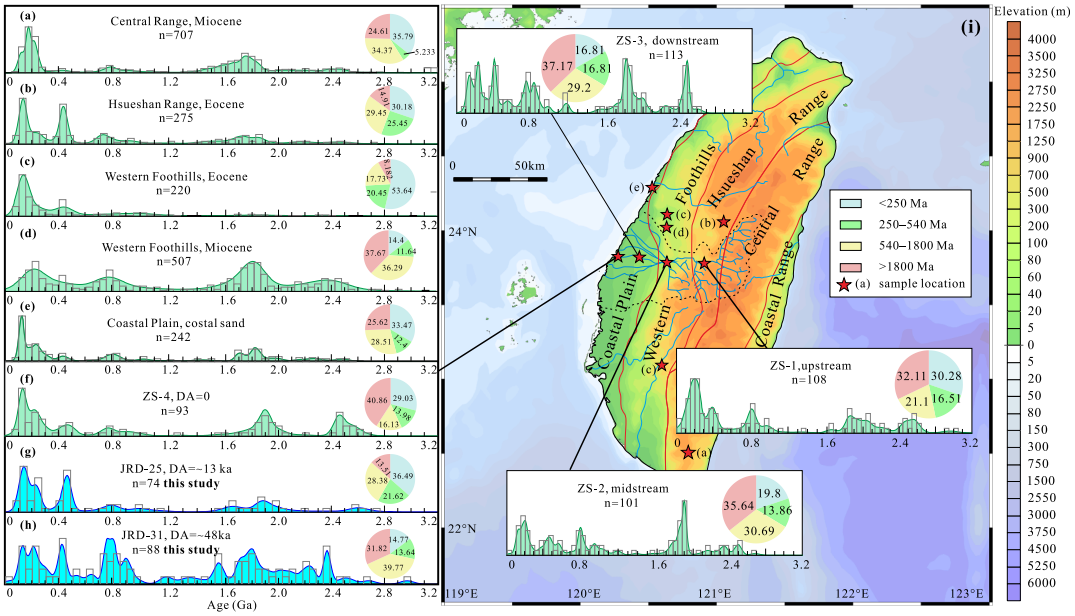

Fig. 5. Kernel density estimation plots for the detrital zircon U—Pb ages of river sand and strata. (a) Miocene strata in Central Range (Zhang et al., 2014, 2017). (b) Eocene strata in Hsueshan Range (Lan et al., 2016). (c) Eocene strata in Western Foothills (Lan et al., 2016; Zhang et al., 2017). (d) Miocene strata in Western Foothills (Lan et al., 2016). (e) coastal sand in Coastal Plain (Chen et al., 2019). (f) modern sand in river mouth of Zhuoshui River, sample ZS-04 (Deng et al., 2017). (g) sample JRD-25 (this study). (h) sample JRD-31 (this study). (i) river sand in different reaches of the Zhuoshui River (Deng et al., 2017).

sandy samples exhibit a low compositional maturity. These samples are plotted close to the end member of lithic fragment in the ternary diagram of quartz-feldspar-lithic fragment (Q-F-L, Fig. 6a), which are different from estuary sediments from large rivers in East Asia such as the Yangtze River and Pearl River (Sun, 1990; Vezzoli et al., 2016). These immature sediments also show fairly different framework grain and heavy mineral compositions from the sediments discharged by the medium-small mountainous rivers in SE China mainland (Shen et al., 2021). Given the unique bedrock lithological, climatic and topographic background in Taiwan, the sediment maturity is not only controlled by parent-rock types (dominated sedimentary and metasedimentary rocks and related recycling processes, Garzanti et al., 2016), but is also influenced by the rapid, dynamic erosion-transport-deposition processes (Deng et al., 2019) during the last sediment cycle.

The outcrop strata in Taiwan have zonal distribution characteristics (Fig. 2a). Upstream bedrocks in the Zhuoshui River basin are mainly composed of relatively higher-grade metamorphic rocks and more strongly diagenetic sedimentary rocks than those in the downstream regions. Therefore, the higher Lms/Ls ratios of the estuarine sediments could reflect more detritus contribution from upper reaches. Additionally, the ZTR index, which reflect the proportion of stable heavy minerals such as zircon, rutile, tourmaline (Hubert, 1962; Morton and Hallsworth, 1999), can also be employed to reveal the provenance information. The older sedimentary strata tend to exhibit higher ZTR index values because unstable heavy minerals (olivine, hornblende, pyrite etc.) can be destroyed during the diagenesis of sedimentary rocks (Garzanti and Andò, 2007). For the Cenozoic strata in Taiwan, the ZTR index values of older strata are higher than those of younger strata (Yokoyama et al., 2007, Fig. S7). As the old strata are distributed in upper reaches, it can be roughly considered that the ZTR index values of the outcrop strata in the Zhuoshui River drainage basin tend to reduce gradually from upstream basin to downstream basin. This tendency is also reflected by the ZTR index values of modern river sands, which show a declined trend from upper to lower reaches in the Zhuoshui River basin (Deng et al., 2016, Fig. S8). Our results indicate that the Holocene samples exhibit high Lms/Ls ratios and ZTR index values than those of last glaciation samples, indicating a sediment supply increase from upstream bedrocks from glacial time to interglacial time.

Detrital zircon geochronology has been widely used in sedimentary provenance analysis due to high stability of zircon crystals in the surface

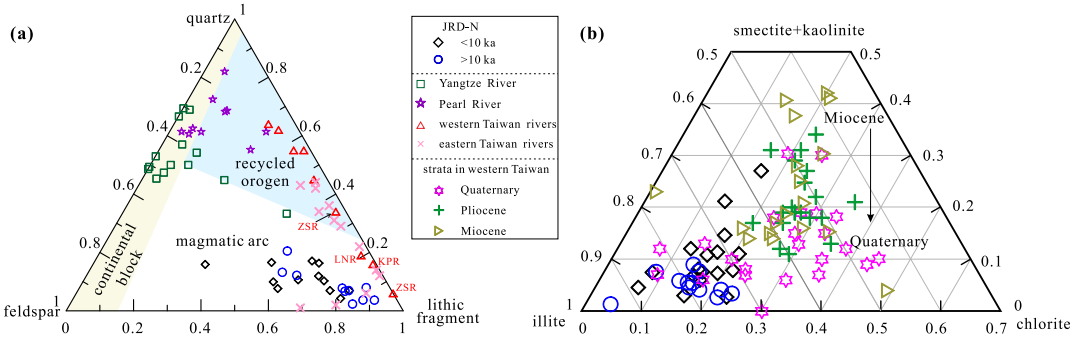

Fig. 6. (a) Ternary diagram of clastic components in the analyzed sand samples. The data of river sands in China mainland are from Sun (1990), the data of Taiwan rivers are from Garzanti and Resentini (2016), the tectonic background fields are from Dickinson (1985). Abbreviation: ZSR-Zhuoshui River, LNR-Laonong River, KPR-Kaoping River. (b) Comparison of clay mineral assemblages among the Core JRD-N samples and the Cenozoic strata samples in Western Taiwan (Nagel et al., 2014).

geological processes (Belousova et al., 2010; Zhang et al., 2021). The samples JRD-31 (~48 ka, Fig. 5h) and JRD-25 (~13 ka, Fig. 5g) in this study and the sample ZS-4 (modern river sand sample, Fig. 5f) in previous study (Deng et al., 2017) are applied to reveal sediment provenance in the last glaciation, deglacial period and Holocene, respectively. The detrital zircon U—Pb age spectrum (KDE plot) of the sample JRD-31 appears high similarity with the Miocene sedimentary strata in the Western Foothills (Fig. 5). Based on the classic multidimensional scaling (MDS) plot, the sample JRD-31 shows affinity to Miocene strata in the Western Foothills and modern river sand samples ZS-2 and ZS-3, which were collected in the Western Foothills and Coastal Plain regions, respectively (Fig. 7a). These results indicate that during the last glaciation, sediments in the Zhuoshui River mouth were mainly contributed by rocks in the downstream basins, including the Coastal Plain and Miocene sedimentary strata in the Western Foothills. By contrast, the detrital zircon age populations of the sample JRD-25 are similar with the Eocene strata signatures in the Hsueshan Range (Fig. 5). Additionally, this affinity is reinforced by the MDS plot results (Fig. 7b). Therefore, during the deglacial period, detritus contribution from bedrocks in the Hsueshan Range, which are located in upper reaches, obviously increased. The sample ZS-4 displays the similar age distribution with Miocene strata in Western Foothills in KED plots, but exhibits a higher proportion of age range < 250 Ma. Note that the upstream rocks, including the Central Range, Hsueshan Range and Eocene strata in Western Foothills appear a high proportion of age range < 250 Ma (Fig. 5). In the MDS plot, the sample ZS-4 shows affinity to other modern river sand samples (Fig. 7c), indicating well-mixed detrital zircon age signatures of the modern river sand from the whole basin. Noteworthily, the coastal sands have similar detrital zircon age signatures with the Central Range, Hsueshan Range and the upstream river sand ZS-01 (Fig. 7). The coastal sands are regarded to be recycled clastic sediments from the western Taiwan rivers (Chen et al., 2019). Therefore, the coastal sand detrital zircon ages would also reveal remarkable contributions from upstream mountains in the Holocene. The detrital zircon U—Pb ages indicate that downstream reaches made major contribution to the river mouth sediments in the last glaciation, while the sediment supply from upper reaches increased obviously in the deglacial period and the Holocene. Collectively, the data of framework grains, heavy minerals and detrital zircon U—Pb geochronology reveal enhanced sediment supply from upstream high-elevation terranes since the deglacial time.

5.1.2. Provenance of mud

Clay mineralogy is employed to constrain the provenance of the muddy sediments from the Zhuoshui River mouth. The clay minerals of the analyzed sediments are composed of more than 60% of illite and more than 20% of chlorite. These sediments show low abundance of kaolinite and infrequent smectite. Compared with the samples for the last glaciation, the Holocene samples exhibit relatively higher abundance of kaolinite and smectite, and lower abundance of chlorite (Fig. 6b). As mentioned above, these clay mineralogical variations also can indicate the provenance changes, rather than chemical weathering intensity variations.

From Miocene to Quaternary outcrop strata in the catchment, the contents of kaolinite and smectite decreased gradually, and the proportion of illite increased (Fig. 6b). Samples of the last glaciation exhibit low abundances of kaolinite and smectite, which is more similar to that of Quaternary strata. The Holocene samples exhibit higher proportion of kaolinite and smectite, implying potential sediment supply from the Miocene strata (Fig. 6b). This variation indicates that during the last glaciation, the source rocks of the discharged sediments of the Zhuoshui River are dominated by those Quaternary strata, while the Neogene strata have made more contribution since the end of last glaciation. This interpretation is also reinforced by the illite crystallinity analysis results.

The illite crystallinity index can indicate degrees of diagenesis and metamorphism in sedimentary or low-grade metamorphic rocks (Bi and Mo, 2004). Usually, older strata exhibit lower illite crystallinity index values due to higher grade diagenesis or metamorphism of the sedimentary strata (Bi and Mo, 2004). Previously published data indicate that the illite crystallinity index values have an increasing trend from the upstream to downstream strata in the Zhuoshui River catchment (Fig. S9, Nagel et al., 2014). Our results show that illite crystallinity index values of the interstadial stage samples (48–32 ka) and Holocene samples are in a low range (Fig. 4 k), indicating relatively high contribution from the upstream basin. By contrast, the LGM samples have relatively high illite crystallinity index values, suggesting increased supply from the downstream bedrock and reduced upstream contribution. Therefore, both sand and mud provenance interpretations favor that in the last glaciation, the Zhuoshui River sediments were mainly contributed by downstream bedrock (Coastal Plain and Western Foothills). The upstream bedrock made more contribution to the river sediments during the deglacial time and the Holocene.

5.2. Potential causes for variations in the sediment supply and provenance

Several potential causes can lead to the sediment supply and provenance change. These include (1) mountainous glaciers extending, (2) variation of fluvial transport ability, (3) sea level change and (4) variation of the river system of the Zhuoshui River.

Firstly, although extents of glaciers can cause variations in sediment provenance in the glacial-interglacial cycles, especially from those high latitude regions (e.g., Jiao et al., 2018; Mariotti et al., 2021), it doesn't apply to the Taiwanese rivers. While the equilibrium line altitude (ELA) in Taiwan was higher than 3000 m (Ono et al., 2005), and the glaciers only distributed in few regions, such as the Hsueshan, Nanhuta and Yushan Mountains (Cui et al., 2002, Fig. 2a). Therefore, the glacier-driving denudation was likely limited in Taiwan during the last glaciation, and it couldn't lead to significant variations in sediment supply and

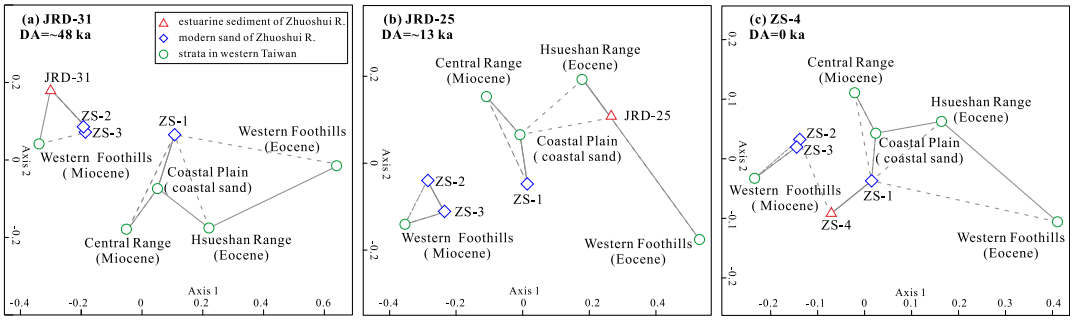

Fig. 7. The classic multidimensional scaling (MDS) plot for detrital zircon U—Pb ages of Taiwan sediments, references are shown in captions of Fig. 5. The MDS analysis is a standard statistical technique. In the MDS plot, the affinity of sediment is positively correlated with distance, solid lines and dashed lines indicate the closest and second closest neighbors, respectively (Vermeesch, 2013; Vermeesch et al., 2016).

transport.

Secondly, rainfall variation-induced river runoff changes and landslides may influence sediment supply and transport processes. In the last glaciation, especially during the LGM, rainfall in Taiwan was much less than the modern precipitation (Yang et al., 2011). The decline of rainfall and runoff, could decrease sediment transport ability. This is indicated by the low sediment flux in the last glaciation (Yang et al., 2017). Previous studies found that during the last glaciation, landslides occurred in the Alishan River basin, a tributary of the Zhuoshui River, and the drainage networks of Alishan River were destroyed. Due to declined erosion and transport ability, runoff hardly down-cut the colluvium. As a result, previous riverbeds, where erosion occurred, were instead dominated by deposition (Hsieh et al., 2018). By contrast, landslides occurred frequently in Taiwan during the deglacial and Holocene periods (Pánek, 2019), which are expected to enhance sediment supply and transport ability and can result in high sediment flux in the Zhuoshui River delta regions. However, we are not able to determine the spatial differences of river runoff and landslides in different reaches of the Zhuoshui River and infer that all these processes hardly influenced the ratios of sediment contribution from each reach in a small mountainous river.

As the study area is located in intensive land-ocean interaction regions, the fluctuation of sea level probably influences the sediment compositions via varying sediment transport pathways, i.e., ocean currents during high level periods, and erosion in incised valley during the low sea level periods. Note that the marine environments around the current Zhuoshui River mouth region lasted for ~5.5 kyr (10 to 4.5 ka, Yang et al., 2017) in the early-mid Holocene, whereas this region was in terrestrial environments for most of the time during the last glaciation. The Taiwan Warm Current, which formed at ~8.4 ka (Li et al., 2012b), could only transport mud sediments but hardly transport sand sediments (Liu et al., 2008a, 2008b; Xu et al., 2009; Shen et al., 2021). Therefore, the marine environments might play a minor role in provenance variation of the core JRD-N sediments. Note that a Holocene sample (JRD-38) exhibits high smectite content (23%). Clay mineralogical data of river sediments from Luzon Island, to south of Taiwan indicate high smectite abundance (~86%, Liu et al., 2009). Therefore, we infer that the Luzon-sourced clays may be transported by branch of the Kuroshio Current to the Zhuoshui river mouth during the high sea level period. Besides, the declining of sea level would result in remarkable incisions in valleys or flood plain, especially in lower reaches, and the provenance of estuarine sediments would vary obviously (e.g., Goodbred Jr et al., 2003; Rittenour et al., 2007; Wang et al., 2008; Sarkar et al., 2009; Wei and Wu, 2011). During the last glaciation, the margin seas retained relatively low sea level, with a lowest level about −140 m in the LGM (Bard et al., 1990, Fig. 3c). Therefore, we infer that the valley and plain in the Zhuoshui River basin underwent incision during the last glaciation. Previous studies suggest that the Pakua fluvial terranes (in Coastal Plain), have the youngest terranes of ~31 ka (Ota et al., 2002; Tsai et al., 2007), indicating the incision time in the last glaciation. The modern Zhuoshui River mouth was previously in flood plain or fluvial channel environment during the last glaciation (Yang et al., 2017). And mount of incised sediments deposited in the location of the core site. Due to the sea level rise in a short time, the stage of incised valley ended at ~12 ka (Yang et al., 2017). With the ending of erosion, the sediment from downstream regions reduced substantially.

The bedrocks in the Zhuoshui River upper reaches are more easily denudated than those in lower reaches (Deng et al., 2020). During the MIS3 stage (58–25 ka), the climate condition in East Asia was similar to that in today (Ren et al., 1996; Wu and Liu, 1996; An and Porter, 1997). Theoretically, the upstream rocks in the Zhuoshui River basin would retain high denudation rate and contributed a lot of sediments in the MIS3 stage, which is inconsistent with the provenance analysis result in this study. Therefore, we favor that the Zhuoshui River drainage system changed, i.e., the upstream river system was not developed during the last glaciation, but it was developed after the LGM by head-ward extend or/and drainage capture. Previous studies suggest that the Dadu River, one of major rivers in western Taiwan (Fig. 2b), captured other drainage basins in the Hsueshan Range region, and was developed from a small mountain-front river to a relatively large catchment river over the last ~40–60 kyr (Simoes et al., 2014). Therefore, we infer that similar capture events occurred in the Zhuoshui River drainage basin after the end of last glaciation.

5.3. The drainage reorganization of the Zhuoshui River since the last glaciation

We note that the clay mineralogical data from the core JRD-S (close to the analyzed core JRD-N in this study, Wan et al., 2020), indicate relatively stable sediment provenance since ca. 23 ka (including 6 mud samples), which are different from our results. We consider that the different results might be due to the different sample resolution in time, the distinct sedimentary environments of the two cores (Yang et al., 2017) and the sediment heterogeneity in this small, dynamic mountainous river (Deng et al., 2019). Further detailed and high-spatiotemporal-resolution investigations are required to better constrain the provenance evolution since the last glaciation. Here, based on our new integrated provenance analysis data from both sands and muds at the Zhuoshui River mouth, we propose a two-stage model for the drainage variation of the small mountainous rivers in Taiwan. In the last glaciation, the Zhuoshui River was likely a small mountain-front river, with a short stream and a small drainage basin. Due to the low sea level, river estuary migrated westward into the modern Taiwan Strait, and incised valleys were developed in lower reaches where the sediments mainly came from (Fig. 8a). After the last glaciation, the upstream basin was expanded due to enhanced physical erosion and possible, drainage capture in high-altitude regions. As a result, the upstream bedrock increasingly contributed sediments to the estuary regions (Fig. 8b).

River drainage evolution can be driven by different mechanisms, mainly including (1) tectonic or morphotectonic controls (e.g., Beard, 1999; Yin and Yu, 2000; Zelilidis, 2000; Moore and Larkin, 2001; Maroukian et al., 2008; Galloway and Whiteaker, 2011) and (2) climatic factors (Lemmen et al., 1994; Bridgland and d'Olier, 1995; Roddaz et al., 2005). Although Taiwan is located in a tectonically active setting and earthquake frequently occurs (Huang et al., 1997; Dadson et al., 2003), there is no evidence of a significant shift of the tectonic regimes (commonly with a million-year timescale) since the last glaciation. Therefore, tectonic events might not be a crucial factor for the drainage reorganization and sediment provenance variations since the last glaciation. Given the obvious differences of sediment provenance between glacial and interglacial periods, we suggest that climate change, particularly changes in rainfall, has played a crucial role in the variation of river system of the Taiwan mountainous rivers since the last glaciation.

Climate in Taiwan has changed significantly since the last glaciation. Global climate change could influence the sea levels (discussed above), and local climate could impact rainfall in Taiwan. The stalagmites $\delta^{18}O$ in China indicated that, due to the oscillation of East Asian summer monsoon, during the MIS3 stage and Holocene, precipitation in East Asia (including Taiwan) was abundant but declined in the LGM (Cosford et al., 2008; Cheng et al., 2016, Fig. 4c). Rainfall can extend the river channel headward, increasing the rills density and causing drainage capture by erosion processes (Tucker and Bras, 2000; Pelletier, 2003). Furthermore, local climate also can influence the vegetation coverage in Taiwan. It has been reported that Taiwanese vegetation types varied significantly since the last glaciation. Specifically, in the central and southern Taiwan, vegetation was dominated by temperature deciduous and conifer mixed forest in the last glaciation, and transformed to warm-temperate and subtropical evergreen forest in the Holocene (Liew et al., 2006; Lee and Liew, 2010). Although vegetation types and densities could vary the dominated erosion types and influence drainage density (Istanbulluoglu and Bras, 2005), whether and how the vegetation

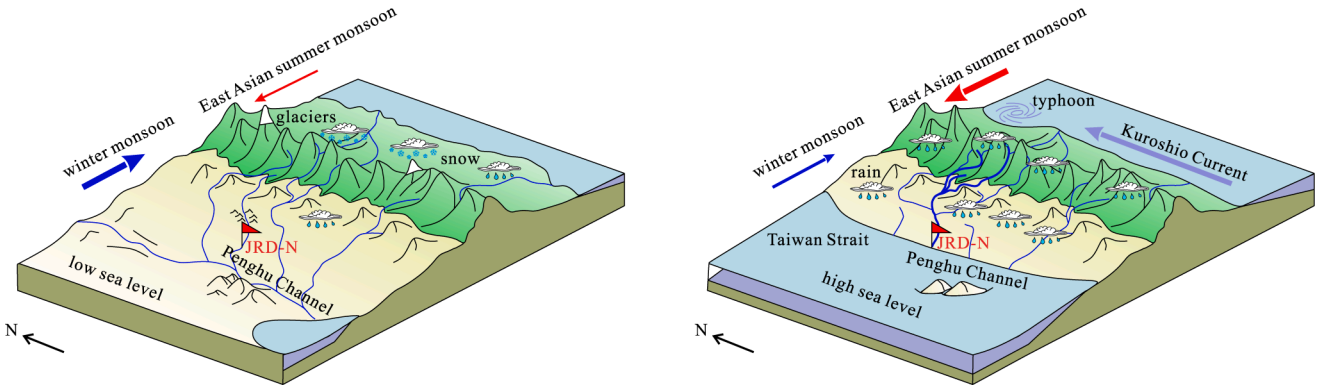

Fig. 8. The schematic model of evolution of mountainous river systems in Taiwan. (a) In glaciation, the river is shorter and with less runoff because of the less rain and weak East Asian summer monsoon. (b) In the interglacial age, the river extends headward and captured other basins in mountainous areas due to heavy rainfalls. The yellow area symbolizes the downstream plain and hills, the green area symbolizes the upstream mountains. (For interpretation of the references to colour in this figure legend, the reader is referred to the web version of this article.)

variations since the last glaciation impact the river drainage basins in Taiwan remain open questions.

5.4. Implications

It is well accepted that the small mountainous rivers in South and East Asia deliver a disproportionately large amounts of sediments to the global ocean (Milliman and Farnsworth, 2011). Those rivers in Taiwan are thought to account for a major source and pathway for sediments in the East Asia continental margin, and Taiwan serves as a key source area for related sediment source to sink studies (Liu et al., 2008a; Liu et al., 2013). The new data in this study indicate variable sediment compositions over time from the Taiwan mountainous rivers since the last glaciation, implying a dynamic, inconstant end-member signature for those sediment provenance analysis, paleoclimatic, paleohydrologic and paleogeographic studies concerning adjacent sediment sinks. Furthermore, this study emphasizes the key role of rainfall, which is driven by global climate change, in landscape evolution dynamics of Earth's surface over millennium timescales. Our findings are expected to be useful to better understand the East Asia land-ocean interactions and the relationships among Earth's spheres during the glacial-interglacial cycles.

6. Conclusions

This study combines framework grain petrographic, clay mineral, heavy mineral and detrital zircon U—Pb age data of drilled core sediments from Zhuoshui River delta in Taiwan and yields the following conclusions:

1. During the last glaciation, the estuarine sediments of the Zhuoshui River were mainly contributed by downstream bedrock, indicated by low proportion of meta-sedimentary lithic fragments, low ZTR index values, low abundance of smectite and kaolinite, high illite crystallinity index values and distribution of detrital zircon U—Pb ages.
2. The increasing meta-sedimentary lithic fragments abundances, ZTR index values, proportion of smectite and kaolinite, reducing illite crystallinity index values and greatly changed distribution of detrital zircon U—Pb ages indicate that the upper reach bedrock increasingly contributed sediments to the estuary of the Zhuoshui River in the Holocene.
3. We suggest that the provenance variations were due to (1) erosion in incised valley during the last glaciation and (2) river system reorganization which caused by headward extension and drainage capture events during the deglacial time. This drainage evolutionary history was most likely related to increasing rainfall resulted from the strengthened East Asian summer monsoon in a warm period.

Declaration of Competing Interest

We declare that we don't have any conflict of interest.

Acknowledgments

This work was funded by the National Natural Science Foundation of China (41806052), Natural Science Foundation of Fujian Province (2017J05067) and Xiamen University Fundamental Research Funds for the Central Universities (20720190097 and 20720190103). Xiamen University supported mutual academic exchange visits to XJ and JTL to carry out the collaboration. The funding for drilling the JRD-N core was provided by the ROC Ministry of Science and Technology under the grant numbers: NSC 99-2611-M-110-005, NSC 100-2611-M-110-013 to JTL. We are grateful to Editor Paul Hesse, Editor in chief Thomas Algeo, Dr. Ruohong Jiao and two anonymous reviewers for their thoughtful reviews that improved this manuscript.

Appendix A. Supplementary data

Supplementary data to this article can be found online at https://doi.org/10.1016/j.palaeo.2021.110759.

References

An, Z.S., Porter, S.C., 1997. Millennial–scale climatic oscillations during the last interglaciation in central China. Geology 25 (7), 603–606. https://doi.org/10.1130/0091–7613(1997)025<0603:MSCODT>2.3.CO;2.

Andersen, T., 2002. Correction of common lead in U–Pb analyses that do not report 204Pb. Chem. Geol. 192, 59–79. https://doi.org/10.1016/S0009–2541(02)00195–X.

Bard, E., Hamelin, B., Fairbanks, R.G., 1990. U–Th ages obtained by mass spectrometry in corals from Barbados: sea level during the past 130,000 years. Nature 346, 456–458.

Beard, J.S., 1999. Evolution of the river systems of the south–west drainage division, Western Australia. J. R. Soc. West. Aust. 82, 147.

Belousova, E.A., Kostitsyn, Y.A., Griffin, W.L., Begg, G.C., O'Reilly, S.Y., Pearson, N.J., 2010. The growth of the continental crust: constraints from zircon Hf–isotope data. Lithos 119, 457–466. https://doi.org/10.1016/j.lithos.2010.07.024.

Bi, X.M., Mo, X.X., 2004. Transition from diagenesis to low–grade metamorphism and related minerals and energy resources. Earth Sci. Front. 11, 287–294 (in Chinese with English abstract).

Biscaye, P.E., 1965. Mineralogy and sedimentation of recent deep–sea clay in the Atlantic Ocean and adjacent seas and oceans. Geol. Soc. Am. Bull. 76, 803–832. https://doi.org/10.1130/00167606(1965)76[803:MASORD]2.0.CO;2.

Böse, M., 2004. Traces of glaciation in the high mountains of Taiwan. In: Developments in Quaternary Sciences, 2. Elsevier, pp. 347–352. https://doi.org/10.1016/S1571–0866(04)80141–6.
Briais, A., Patriat, P., Tapponnier, P., 1993. Updated interpretation of magnetic anomalies and seafloor spreading stages in the South China Sea: Implications for the Tertiary tectonics of Southeast Asia. J. Geophys. Res. Solid Earth 98, 6299–6328. https://doi.org/10.1029/92JB02280.
Bridgland, D.R., d'Olier, B., 1995. The Pleistocene evolution of the Thames and Rhine drainage systems in the southern North Sea Basin. Geol. Soc. Lond., Spec. Publ. 96, 27–45. https://doi.org/10.1144/GSL.SP.1995.096.01.04.
Chai, B.H., 1972. Structure and tectonic evolution of Taiwan. Am. J. Sci. 272 (5), 389–422.
Chang, L.H., Chen, M.Y., Jin, W., Li, S.C., Yu, J.J., 2010. Transparent Mineral Sheet Identification Manual. Geology Press, Beijing, China, pp. 250–256 (in Chinese).
Chen, C.H., Wang, C.H., 1995. Explanatory Notes for the Metamorphic Facies Map of Taiwan.
Chen, H.F., Wen, S.Y., Song, S.R., Yang, T.N., Lee, T.Q., Lin, S.F., Yu, P.S., 2012. Strengthening of paleo-typhoon and autumn rainfall in Taiwan corresponding to the Southern Oscillation at late Holocene. J. Quat. Sci. 27, 964–972. https://doi.org/10.1002/jqs.2590.
Chen, Q., Liu, Z., Kissel, C., 2017a. Clay mineralogical and geochemical proxies of the East Asian summer monsoon evolution in the South China Sea during Late Quaternary. Sci. Rep. 7, 42083. https://doi.org/10.1038/srep42083.
Chen, W.H., Huang, C.Y., Yan, Y., Dilek, Y., Chen, D., Wang, M.H., Zhang, X., Lan, Q., Yu, M., 2017b. Stratigraphy and provenance of forearc sequences in the Lichi Mélange, Coastal Range: Geological records of the active Taiwan arc–continent collision. J. Geophys. Res. Solid Earth 122, 7408–7436. https://doi.org/10.1002/2017JB014378.
Chen, C.H., Lee, C.Y., Lin, J.W., Chu, M.F., 2019. Provenance of sediments in western Foothills and Hsuehshan Range (Taiwan): A new view based on the EMP monazite versus LA–ICPMS zircon geochronology of detrital grains. Earth Sci. Rev. 190, 224–246. https://doi.org/10.1016/j.earscirev.2018.12.015.
Cheng, H., Edwards, R.L., Sinha, A., Spötl, C., Yi, L., Chen, S., Zhang, H., 2016. The Asian monsoon over the past 640,000 years and ice age terminations. Nature 534 (7609), 640–646. https://doi.org/10.1038/nature18591.
Chikita, K.A., Kemnitz, R., Kumai, R., 2002. Characteristics of sediment discharge in the subarctic Yukon River, Alaska. Catena 48, 235–253. https://doi.org/10.1016/S0341–8162(02)00032–2.
Clemens, S.C., Holbourn, A., Kubota, Y., Lee, K.E., Liu, Z., Chen, G., Fox-Kemper, B., 2018. Precession-band variance missing from East Asian monsoon runoff. Nat. Commun. 9 (1), 1–12. https://doi.org/10.1038/s41467-018-05814-0.
Cosford, J., Qing, H., Yuan, D., Zhang, M., Holmden, C., Patterson, W., Hai, C., 2008. Millennial–scale variability in the Asian monsoon: Evidence from oxygen isotope records from stalagmites in southeastern China. Palaeogeogr. Palaeoclimatol. Palaeoecol. 266, 3–12. https://doi.org/10.1016/j.palaeo.2008.03.029.
Cui, Z., Yang, C., Liu, G., Zhang, W., Wang, S., Sung, Q., 2002. The Quaternary glaciation of Shesan Mountain in Taiwan and glacial classification in monsoon areas. Quat. Int. 97, 147–153. https://doi.org/10.1016/S1040–6182(02)00060–5.
Dadson, S.J., Hovius, N., Chen, H., Dade, W.B., Hsieh, M.L., Willett, S.D., Lague, D., 2003. Links between erosion, runoff variability and seismicity in the Taiwan orogen. Nature 426, 648–651. https://doi.org/10.1038/nature02150.
Dadson, S.J., Hovius, N., Chen, H., Dade, W.B., Lin, J.C., Hsu, M.L., Stark, C.P., 2004. Earthquake–triggered increase in sediment delivery from an active mountain belt. Geology 32, 733–736. https://doi.org/10.1130/G20639.1.
Dadson, S., Hovius, N., Pegg, S., Dade, W.B., Horng, M.J., Chen, H., 2005. Hyperpycnal river flows from an active mountain belt. J. Geophys. Res. Earth Surf. 110 https://doi.org/10.1029/2004JF000244.
Deng, B., Zhang, J., Wu, Y., 2006. Recent sediment accumulation and carbon burial in the East China Sea. Glob. Biogeochem. Cycles 20. https://doi.org/10.1029/2005GB002559.
Deng, K., Yang, S.Y., Wang, Z.B., Li, C., Bi, L., Zhang, Y.B., Liu, Z.Q., 2016. Detrital heavy, mineral assemblages in the river sediments from Taiwan and its implications for sediment provenance. Acta Sedimentol. Sin. 34, 531–542 (in Chinese with English abstract).
Deng, K., Yang, S., Li, C., Su, N., Bi, L., Chang, Y.P., Chang, S.C., 2017. Detrital zircon geochronology of river sands from Taiwan: Implications for sedimentary provenance of Taiwan and its source link with the east China mainland. Earth Sci. Rev. 164, 31–47. https://doi.org/10.1016/j.earscirev.2016.10.015.
Deng, K., Yang, S., Bi, L., Chang, Y.P., Su, N., Frings, P., Xie, X., 2019. Small dynamic mountainous rivers in Taiwan exhibit large sedimentary geochemical and provenance heterogeneity over multi–spatial scales. Earth Planet. Sci. Lett. 505, 96–109. https://doi.org/10.1016/j.epsl.2018.10.012.
Deng, K., Yang, S., Blanckenburg, F., Wittmann, H., 2020. Denudation rate changes along a fast-eroding mountainous river with slate headwaters in Taiwan from 10Be (meteoric)/9Be ratios. J. Geophys. Res. Earth Surf. 125 https://doi.org/10.1029/2019JF005251 e2019JF005251.
Dickinson, W.R., 1985. Interpreting provenance relations from detrital modes of sandstones. In: Zuffa, G.G. (Ed.), Provenance of Arenites. Reidel, Dordrecht, pp. 333–336.
Dou, Y., Yang, S., Lim, D.I., Jung, H.S., 2015. Provenance discrimination of last deglacial and Holocene sediments in the southwest of Cheju Island, East China Sea. Palaeogeogr. Palaeoclimatol. Palaeoecol. 422, 25–35. https://doi.org/10.1016/j.palaeo.2015.01.016.
Dou, Y., Yang, S., Shi, X., Clift, P.D., Liu, S., Liu, J., Zhao, Y., 2016. Provenance weathering and erosion records in southern Okinawa Trough sediments since 28 ka: geochemical and Sr–Nd–Pb isotopic evidences. Chem. Geol. 425, 93–109. https://doi.org/10.1016/j.chemgeo.2016.01.029.
Galloway, W.E., Whiteaker, T.L., Ganey-Curry, P., 2011. History of Cenozoic North American drainage basin evolution, sediment yield, and accumulation in the Gulf of Mexico basin. Geosphere 7, 938–973. https://doi.org/10.1130/GES00647.1.
Garzanti, E., Andò, S., 2007. Heavy mineral concentration in modern sands: implications for provenance interpretation. Dev. Sedimentol. 58, 517–545. https://doi.org/10.1016/S0070–4571(07)58020–9.
Garzanti, E., Resentini, A., 2016. Provenance control on chemical indices of weathering (Taiwan river sands). Sediment. Geol. 336, 81–95. https://doi.org/10.1016/j.sedgeo.2015.06.013.
Garzanti, E., Al-Juboury, A.I., Zoleikhaei, Y., Vermeesch, P., Jotheri, J., Akkoca, D.B., Vezzoli, G., 2016. The Euphrates-Tigris-Karun river system: Provenance, recycling and dispersal of quartz-poor foreland-basin sediments in arid climate. Earth Sci. Rev. 162, 107–128. https://doi.org/10.1016/j.earscirev.2016.09.009.
Gehrels, G., Valencia, V., Pullen, A., 2006. Detrital zircon geochronology by laser–ablation multicollector ICPMS at the Arizona LaserChron Center. The Paleontol. Soc. Papers 12, 67–76. https://doi.org/10.1017/S1089332600001352.
Gehrels, G.E., Valencia, V.A., Ruiz, J., 2008. Enhanced precision, accuracy, efficiency, and spatial resolution of U-Pb ages by laser ablation–multicollector–inductively coupled plasma–mass spectrometry. Geochem. Geophys. Geosyst. 9 https://doi.org/10.1029/2007GC001805.
Goodbred Jr., S.L., Kuehl, S.A., Steckler, M.S., Sarker, M.H., 2003. Controls on facies distribution and stratigraphic preservation in the Ganges–Brahmaputra delta sequence. Sediment. Geol. 155, 301–316. https://doi.org/10.1016/S0037–0738(02)00184–7.
Han, Y.S., Zhang, H., Tseng, Y.H., Shen, M.L., 2012. Larval Japanese eel (*Anguilla japonica*) as sub-surface current bio-tracers on the East Asia continental shelf. Fish. Oceanogr. 21, 281–290. https://doi.org/10.1111/j.1365–2419.2012.00624.x.
Hebenstreit, R., Böse, M., Murray, A., 2006. Late Pleistocene and early Holocene glaciations in Taiwanese mountains. Quat. Int. 147, 76–88. https://doi.org/10.1016/j.quaint.2005.09.009.
Hilton, R.G., Galy, A., Hovius, N., Chen, M.C., Horng, M.J., Chen, H., 2008. Tropical–cyclone–driven erosion of the terrestrial biosphere from mountains. Nat. Geosci. 1, 759–762. https://doi.org/10.1038/ngeo333.
Ho, C.S., 1986. A synthesis of the geologic evolution of Taiwan. Tectonophysics 125, 1–16. https://doi.org/10.1016/0040–1951(86)90004–1.
Ho, C.S., Hsu, M.Y., Jen, L.S., Fong, G.S., 1964. Geology and coal resources of the northern coastal area of Taiwan. Bull. Geol. Survey Taiwan 15, 1–23.
Holtzapffel, T., 1985. Les minéraux argileux. In: Préparation. Analyse diffractométrique et détermination. Publication–Société géologique du Nord, p. 12.
Hsieh, M.L., Hogg, A., Kang, S.C., Chou, C.Y., 2018. The preservation of last-glacial (> 50 to 40 ka) colluvium on low-relief surfaces in Alishan, an actively uplifting mountain in southwestern Taiwan. Geomorphology 322, 159–174. https://doi.org/10.1016/j.geomorph.2018.08.041.
Hsu, W.H., Byrne, T.B., Ouimet, W., Lee, Y.H., Chen, Y.G., Soest, M.V., Hodges, K., 2016. Pleistocene onset of rapid, punctuated exhumation in the eastern Central Range of the Taiwan orogenic belt. Geology 44, 719–722. https://doi.org/10.1130/G37914.1.
Huang, C.Y., 1986. Oligocene and miocene stratigraphy of the Kuohsing area, central Taiwan. Acta Geol. Taiwan. 281–318 (in Chinese).
Huang, T.C., Ting, J.S., 1979. Calcareous nannofossils succession from the Oligo–Miocene Peikangchi section and revised stratigraphic correlation between northern and central Taiwan. Proceed. Geol. Soc. China 22, 105–120 (in Chinese with English abstract).
Huang, C.Y., Yuan, P.B., Song, S.R., Lin, C.W., Wang, C., Chen, M.T., Karp, B., 1995. Tectonics of short-lived intra-arc basins in the arc-continent collision terrane of the Coastal Range, eastern Taiwan. Tectonics 14, 19–38. https://doi.org/10.1029/94TC02452.
Huang, C.Y., Wu, W.Y., Chang, C.P., Tsao, S., Yuan, P.B., Lin, C.W., Xia, K.Y., 1997. Tectonic evolution of accretionary prism in the arc–continent collision terrane of Taiwan. Tectonophysics 281, 31–51. https://doi.org/10.1016/S0040–1951(97)00157–1.
Huang, C.Y., Yen, Y., Zhao, Q., Lin, C.T., 2012. Cenozoic stratigraphy of Taiwan: window into rifting, stratigraphy and paleoceanography of South China Sea. Chin. Sci. Bull. 57, 3130–3149. https://doi.org/10.1007/s11434–012–5349–y.
Hubert, J.F., 1962. A zircon–tourmaline–rutile maturity index and the interdependence of the composition of heavy mineral assemblages with the gross composition and texture of sandstones. J. Sediment. Res. 32, 440–450. https://doi.org/10.1306/74D70CE5–2B21–11D7–8648000102C1865D.
Istanbulluoglu, E., Bras, R.L., 2005. Vegetation-modulated landscape evolution: Effects of vegetation on landscape processes, drainage density, and topography. J. Geophys. Res. Earth Surf. 110 (F2) https://doi.org/10.1029/2004JF000249.
Jian, Z., Wang, P., Saito, Y., Wang, J., Pflaumann, U., Oba, T., Cheng, X., 2000. Holocene variability of the Kuroshio current in the Okinawa Trough, northwestern Pacific Ocean. Earth Planet. Sci. Lett. 184, 305–319. https://doi.org/10.1016/S0012–821X(00)00321–6.
Jian, X., Weislogel, A., Pullen, A., 2019. Triassic sedimentary filling and closure of the eastern Paleo-Tethys Ocean: new insights from detrital zircon geochronology of Songpan-Ganzi, Yidun, and West Qinling flysch in eastern Tibet. Tectonics 38, 767–787. https://doi.org/10.1029/2018TC005300.
Jian, X., Zhang, W., Yang, S., Kao, S.J., 2020. Climate-dependent sediment composition and transport of mountainous rivers in tectonically stable, subtropical East Asia. Geophys. Res. Lett. 47 https://doi.org/10.1029/2019GL086150 e2019GL086150.
Jiao, R., Herman, F., Beyssac, O., Adatte, T., Cox, S.C., Nelson, F.E., Neil, H.L., 2018. Erosion of the Southern Alps of New Zealand during the last deglaciation. Geology 46, 975–978. https://doi.org/10.1130/G45160.1.

John, B.M., Zhou, X.H., Li, J.L., 1990. Formation and tectonic evolution of southeastern China and Taiwan: isotopic and geochemical constraints. Tectonophysics 183, 145–160. https://doi.org/10.1016/0040–1951(90)90413–3.
Kao, S.J., Milliman, J.D., 2008. Water and sediment discharge from small mountainous rivers, Taiwan: the roles of lithology, episodic events, and human activities. The J. Geol. 116, 431–448.
Kao, S.J., Chan, S.C., Kuo, C.H., Liu, K.K., 2005a. Transport–dominated sediment loading in Taiwanese rivers: a case study from the Ma–an Stream. The J. Geol. 113, 217–225. https://doi.org/10.1086/427670.
Kao, S.J., Lee, T.Y., Milliman, J.D., 2005b. Calculating highly fluctuated suspended sediment fluxes from mountainous rivers in Taiwan. Terr. Atmos. Ocean. Sci. 16, 653.
Kao, S.J., Roberts, A.P., Hsu, S.C., Chang, Y.P., Lyons, W.B., Chen, M.T., 2006a. Monsoon forcing, hydrodynamics of the Kuroshio Current, and tectonic effects on sedimentary carbon and sulfur cycling in the Okinawa Trough since 90 ka. Geophys. Res. Lett. 33 https://doi.org/10.1029/2005GL025154.
Kao, S.J., Wu, C.R., Hsin, Y.C., Dai, M., 2006b. Effects of sea level change on the upstream Kuroshio Current through the Okinawa Trough. Geophys. Res. Lett. 33 https://doi.org/10.1029/2006GL026822.
Kao, S.J., Jan, S., Hsu, S.C., Lee, T.Y., Dai, M., 2008. Sediment budget in the taiwan strait with high fluvial sediment inputs from mountainous rivers: new observations and synthesis. Terr. Atmos. Ocean. Sci. 19 https://doi.org/10.3319/TAO.2008.19.5.525 (Oc).
Kao, S.J., Huang, J.C., Lee, T.Y., Liu, C.C., Walling, D.E., 2011. The changing rainfall–runoff dynamics and sediment response of small mountainous rivers in Taiwan under a warming climate. In: Sediment Problems and Sediment Management in Asian River Basins (IAHS Publ 349).
Lan, Q., Yan, Y., Huang, C.Y., Santosh, M., Shan, Y.H., Chen, W., Qian, K., 2016. Topographic architecture and drainage reorganization in Southeast China: Zircon U–Pb chronology and Hf isotope evidence from Taiwan. Gondwana Res. 36, 376–389. https://doi.org/10.1016/j.gr.2015.07.008.
Lee, C.Y., Liew, P.M., 2010. Late Quaternary vegetation and climate changes inferred from a pollen record of Dongyuan Lake in southern Taiwan. Palaeogeogr. Palaeoclimatol. Palaeoecol. 287, 58–66. https://doi.org/10.1016/j.palaeo.2010.01.015.
Lee, J., Liu, J.T., Hung, C.C., Lin, S., Du, X., 2016. River plume induced variability of suspended particle characteristics. Mar. Geol. 380, 219–230. https://doi.org/10.1016/j.margeo.2016.04.014.
Leithold, E.L., Blair, N.E., Perkey, D.W., 2006. Geomorphologic controls on the age of particulate organic carbon from small mountainous and upland rivers. Glob. Biogeochem. Cycles 20. https://doi.org/10.1029/2005GB002677.
Lemmen, D.S., Duk-Rodkin, A., Bednarski, J.M., 1994. Late glacial drainage systems along the northwestern margin of the Laurentide Ice Sheet. Quat. Sci. Rev. 13, 805–828. https://doi.org/10.1016/0277–3791(94)90003–5.
Li, C., Zhou, Z., Li, J., Chen, H., Geng, J., Li, H., 2007. Precollisional tectonics and terrain amalgamation offshore southern Taiwan: Characterizations from reflection seismic and potential field data. Sci. China Ser. D Earth Sci. 50, 897–908.
Li, C., Shi, X., Kao, S., Chen, M., Liu, Y., Fang, X., Qiao, S., 2012a. Clay mineral composition and their sources for the fluvial sediments of Taiwanese rivers. Chin. Sci. Bull. 57, 673–681. https://doi.org/10.1007/s11434–011–4824–1.
Li, X.Y., Jian, Z.M., Shi, X.F., Liu, S.F., 2012b. Holocene foraminifera from the mud area of the inner shelf, east China Sea and their paleoenvironmental significance. Mar. Geol. Quat. Geol. 32, 61–71 (in Chinese with English Abstract).
Li, C., Yang, S., Zhao, J.X., Dosseto, A., Bi, L., Clark, T.R., 2016. The time scale of river sediment source–to–sink processes in East Asia. Chem. Geol. 446, 138–146. https://doi.org/10.1016/j.chemgeo.2016.06.012.
Li, J., Liu, S., Feng, X., Sun, X., Shi, X., 2017. Major and trace element geochemistry of the mid–Bay of Bengal surface sediments: implications for provenance. Acta Oceanol. Sin. 36, 82–90 (in Chinese with English abstract).
Li, J., Liu, S., Shi, X., Zhang, H., Fang, X., Chen, M.T., Khokiattiwong, S., 2018. Clay minerals and Sr–Nd isotopic composition of the Bay of Bengal sediments: implications for sediment provenance and climate control since 40 ka. Quat. Int. 493, 50–58. https://doi.org/10.1016/j.quaint.2018.06.044.
Liew, P.M., Huang, S.Y., Kuo, C.M., 2006. Pollen stratigraphy, vegetation and environment of the last glacial and Holocene—a record from Toushe Basin, central Taiwan. Quat. Int. 147, 16–33. https://doi.org/10.1016/j.quaint.2005.09.003.
Liu, T.K., Hsieh, S., Chen, Y.G., Chen, W.S., 2001. Thermo–kinematic evolution of the Taiwan oblique–collision mountain belt as revealed by zircon fission track dating. Earth Planet. Sci. Lett. 186, 45–56. https://doi.org/10.1016/S0012–821X(01)00232–1.
Liu, J.P., Liu, C.S., Xu, K.H., Milliman, J.D., Chiu, J.K., Kao, S.J., Lin, S.W., 2008a. Flux and fate of small mountainous rivers derived sediments into the Taiwan Strait. Mar. Geol. 256, 65–76. https://doi.org/10.1016/j.margeo.2008.09.007.
Liu, Z., Tuo, S., Colin, C., Liu, J.T., Huang, C.Y., Selvaraj, K., Chen, Z., 2008b. Detrital fine–grained sediment contribution from Taiwan to the northern South China Sea and its relation to regional ocean circulation. Mar. Geol. 255 (3–4), 149–155. https://doi.org/10.1016/j.margeo.2008.08.003.
Liu, Z., Zhao, Y., Colin, C., Siringan, F.P., Wu, Q., 2009. Chemical weathering in Luzon, Philippines from clay mineralogy and major–element geochemistry of river sediments. Appl. Geochem. 24, 2195–2205. https://doi.org/10.1016/j.apgeochem.2009.09.025.
Liu, J.T., Kao, S.J., Huh, C.A., Hung, C.C., 2013. Gravity flows associated with flood events and carbon burial: Taiwan as instructional source area. Annu. Rev. Mar. Sci. 5, 47–68. https://doi.org/10.1146/annurev–marine–121211–172307.
Lin, C.T., Harris, R., Sun, W.D., Zhang, G.L., 2019. Geochemical and geochronological constraints on the origin and emplacement of the East Taiwan Ophiolite. Geochem. Geophys. Geosyst. 20, 2110–2133. https://doi.org/10.1029/2018GC007902.
Ludwig, K.R., 2012. A Geochronological Toolkit for Microsoft Excel, 5. Berkeley Geochronology Center Special Publication, p. 75.
Ludwig, W., Probst, J.L., 1998. River sediment discharge to the oceans; present-day controls and global budgets. Am. J. Sci. 298, 265–295. https://doi.org/10.2475/ajs.298.4.265.
Lyons, W.B., Nezat, C.A., Carey, A.E., Hicks, D.M., 2002. Organic carbon fluxes to the ocean from high–standing islands. Geology 30, 443–446. https://doi.org/10.1130/0091–7613(2002)030<0443:OCFTTO>2.0.CO;2.
Malavieille, J., Lallemand, S.E., Dominguez, S., Deschamps, A., Lu, C.Y., Liu, C.S., Crew, A.S., 2002. Arc–continent collision in Taiwan: New marine observations and tectonic evolution. Special Papers Geol. Soc. Am. 187–211.
Mange, M.A., Maurer, H.F.W., 1992. Heavy Minerals in Colour. Chapman and Hall, London, UK, pp. 39–134.
Mariotti, A., Blard, P.H., Charreau, J., Toucanne, S., Jorry, S.J., Molliex, S., Keddadouche, K., 2021. Nonlinear forcing of climate on mountain denudation during glaciations. Nat. Geosci. 14, 16–22. https://doi.org/10.1038/s41561–020–00672–2.
Maroukian, H., Gaki-Papanastassiou, K., Karymbalis, E., Vouvalidis, K., Pavlopoulos, K., Papanastassiou, D., Albanakis, K., 2008. Morphotectonic control on drainage network evolution in the Perachora Peninsula, Greece. Geomorphology 102, 81–92. https://doi.org/10.1016/j.geomorph.2007.07.021.
Mei, H., Jian, X., Zhang, W., Fu, H., Zhang, S., 2021. Behavioral differences between weathering and pedogenesis in a subtropical humid granitic terrain: Implications for chemical weathering intensity evaluation. Catena 203, 105368. https://doi.org/10.1016/j.catena.2021.105368.
Meybeck, M., Laroche, L., Dürr, H.H., Syvitski, J.P.M., 2003. Global variability of daily total suspended solids and their fluxes in rivers. Glob. Planet. Chang. 39, 65–93. https://doi.org/10.1016/S0921–8181(03)00018–3.
Milliman, J.D., Farnsworth, K.L., 2011. River Discharge to the Coastal Ocean: A Global Synthesis. Cambridge University Press, p. 384.
Milliman, J.D., Meade, R.H., 1983. World–wide delivery of river sediment to the oceans. The J. Geol. 91, 1–21. https://doi.org/10.1086/628741.
Milliman, J.D., Syvitski, J.P.M., 1992. Geomorphic/tectonic control of sediment discharge to the ocean: The importance of small mountainous rivers. J. Geol. 100, 525–544. https://doi.org/10.1086/629606.
Milliman, J.D., Beardsley, R.C., Zuo-Sheng, Y., Limeburner, R., 1985a. Modern Huanghe–derived muds on the outer shelf of the East China Sea: identification and potential transport mechanisms. Cont. Shelf Res. 4, 175–188. https://doi.org/10.1016/0278–4343(85)90028–7.
Milliman, J.D., Huang-Ting, S., Zuo-Sheng, Y., Mead, R.H., 1985b. Transport and deposition of river sediment in the Changjiang estuary and adjacent continental shelf. Cont. Shelf Res. 4, 37–45. https://doi.org/10.1016/0278–4343(85)90020–2.
Milliman, J.D., Lin, S.W., Kao, S.J., Liu, J.P., Liu, C.S., Chiu, J.K., Lin, Y.C., 2007. Short–term changes in seafloor character due to flood–derived hyperpycnal discharge: Typhoon Mindulle, Taiwan, July 2004. Geology 35, 779–782. https://doi.org/10.1130/G23760A.1.
Milliman, J.D., Lee, T.Y., Huang, J.C., Kao, S.J., 2017. Impact of catastrophic events on small mountainous rivers: Temporal and spatial variations in suspended–and dissolved–solid fluxes along the Choshui River, central western Taiwan, during typhoon Mindulle, July 2–6, 2004. Geochim. Cosmochim. Acta 205, 272–294. https://doi.org/10.1016/j.gca.2017.02.015.
Moore, A.E., Larkin, P.A., 2001. Drainage evolution in south–central Africa since the breakup of Gondwana. S. Afr. J. Geol. 104, 47–68. https://doi.org/10.2113/104.1.47.
Morton, A.C., Hallsworth, C.R., 1999. Processes controlling the composition of heavy mineral assemblages in sandstones. Sediment. Geol. 124, 3–29. https://doi.org/10.1016/S0037–0738(98)00118–3.
Nagel, S., Castelltort, S., Garzanti, E., Lin, A.T., Willett, S.D., Mouthereau, F., Adatte, T., 2014. Provenance evolution during arc–continent collision: sedimentary petrography of Miocene to Pleistocene sediments in the western foreland basin of Taiwan. J. Sediment. Res. 84, 513–528. https://doi.org/10.2110/jsr.2014.44.
Ono, Y., Aoki, T., Hasegawa, H., Dali, L., 2005. Mountain glaciation in Japan and Taiwan at the global Last Glacial Maximum. Quat. Int. 138, 79–92. https://doi.org/10.1016/j.quaint.2005.02.007.
Ota, Y., Shyu, J.B.H., Chen, Y.G., Hsieh, M.L., 2002. Deformation and age of fluvial terraces south of the Choushui River, central Taiwan, and their tectonic implications. Western Pacific Earth Sci. 2, 251–260.
Pánek, T., 2019. Landslides and Quaternary climate changes—The state of the art. Earth Sci. Rev. 196, 102871 https://doi.org/10.1016/j.earscirev.2019.05.015.
Pelletier, J.D., 2003. Drainage basin evolution in the Rainfall Erosion Facility: dependence on initial conditions. Geomorphology 53, 183–196. https://doi.org/10.1016/S0169–555X(02)00353–7.
Postma, H., 1988. Physical and Chemical Oceanographic Aspects of Continental Shelves. Elsevier, Amsterdam, pp. 5–37.
Ren, J.Z., Ding, Z.L., Liu, D.S., Sun, J.M., Zhou, X.Q., 1996. Climatic changes on millennial time scale:evidence from a high resolution loess record. Sci. China (Series D) 385–391.
Rittenour, T.M., Blum, M.D., Goble, R.J., 2007. Fluvial evolution of the lower Mississippi River valley during the last 100 ky glacial cycle: Response to glaciation and sea–level change. Geol. Soc. Am. Bull. 119, 586–608. https://doi.org/10.1130/B25934.1.
Roddaz, M., Viers, J., Brusset, S., Baby, P., Hérail, G., 2005. Sediment provenances and drainage evolution of the Neogene Amazonian foreland basin. Earth Planet. Sci. Lett. 239, 57–78. https://doi.org/10.1016/j.epsl.2005.08.007.

Sarkar, A., Sengupta, S.M.J.M., McArthur, J.M., Ravenscroft, P., Bera, M.K., Bhushan, R., Agrawal, S., 2009. Evolution of Ganges–Brahmaputra western delta plain: clues from sedimentology and carbon isotopes. Quat. Sci. Rev. 28, 2564–2581. https://doi.org/10.1016/j.quascirev.2009.05.016.

Seierstad, I.K., Abbott, P.M., Bigler, M., Blunier, T., Bourne, A.J., Brook, E., Vinther, B. M., 2014. Consistently dated records from the Greenland GRIP, GISP2 and NGRIP ice cores for the past 104 ka reveal regional millennial–scale δ18O gradients with possible Heinrich event imprint. Quat. Sci. Rev. 106, 29–46. https://doi.org/10.1016/j.quascirev.2014.10.032.

Seno, T., Stein, S., Gripp, A.E., 1993. A model for the motion of the Philippine Sea plate consistent with NUVEL-1 and geological data. J. Geophys. Res. Solid Earth 98, 17941–17948. https://doi.org/10.1029/93JB00782.

Shen, X., Jian, X., Li, C., Liu, J.T., Chang, Y.P., Zhang, S., Zhang, W., 2021. Submarine topography–related spatial variability of the southern Taiwan Strait sands (East Asia). Mar. Geol. 436, 106495 https://doi.org/10.1016/j.margeo.2021.106495.

Shi, Y., Gao, J.H., Sheng, H., Du, J., Jia, J.J., Wang, Y.P., Chen, Y.N., 2019. Cross-front sediment transport induced by quick oscillation of the yellow sea warm current: evidence from the sedimentary record. Geophys. Res. Lett. 46, 226–234. https://doi.org/10.1029/2018GL080751.

Simoes, M., Chen, Y.G., Shinde, D.P., Singhvi, A.K., 2014. Lateral variations in the long-term slip rate of the Chelungpu fault, Central Taiwan, from the analysis of deformed fluvial terraces. J. Geophys. Res. Solid Earth 119, 3740–3766. https://doi.org/10.1002/2013JB010057.

Sláma, J., Košler, J., Condon, D.J., Crowley, J.L., Gerdes, A., Hanchar, J.M., Schaltegger, U., 2008. Plešovice zircon—a new natural reference material for U–Pb and Hf isotopic microanalysis. Chem. Geol. 249, 1–35. https://doi.org/10.1016/j.chemgeo.2007.11.005.

Sun, B.Y., 1990. Detrital mineral assemblages in the Huanghe, Changjiang and Zhujiang River delta sediment. Mar. Geol. Quat. Geol. 10, 23–34 (in Chinese with English abstract).

Sun, X.G., Fang, M., Huang, W., 2000. Spatial and temporal variations in suspended particulate matter transport on the Yellow Sea and the East China Sea shelf. Oceanol. Limnol. Sinica 31, 581–587 (in Chinese with English abstract).

Tarazón, J.A., Batalla, R.J., Vericat, D., Balasch, J.C., 2010. Rainfall, runoff and sediment transport relations in a mesoscale mountainous catchment: The River Isábena (Ebro basin). Catena 82, 23–34. https://doi.org/10.1016/j.catena.2010.04.005.

Thomas, H., Bozec, Y., Elkalay, K., De Baar, H.J., 2004. Enhanced open ocean storage of CO_2 from shelf sea pumping. Science 304, 1005–1008. https://doi.org/10.1126/science.1095491.

Tsai, H., Hseu, Z.Y., Huang, W.S., Chen, Z.S., 2007. Pedogenic approach to resolving the geomorphic evolution of the Pakua river terraces in central Taiwan. Geomorphology 83, 14–28. https://doi.org/10.1016/j.geomorph.2006.06.006.

Tucker, G.E., Bras, R.L., 2000. A stochastic approach to modeling the role of rainfall variability in drainage basin evolution. Water Resour. Res. 36, 1953–1964. https://doi.org/10.1029/2000WR900065.

Vermeesch, P., 2012. On the visualisation of detrital age distributions. Chem. Geol. 312, 190–194. https://doi.org/10.1016/j.chemgeo.2012.04.021.

Vermeesch, P., 2013. Multi–sample comparison of detrital age distributions. Chem. Geol. 341, 140–146. https://doi.org/10.1016/j.chemgeo.2013.01.010.

Vermeesch, P., Resentini, A., Garzanti, E., 2016. An R package for statistical provenance analysis. Sediment. Geol. 336, 14–25. https://doi.org/10.1016/j.sedgeo.2016.01.009.

Vezzoli, G., Garzanti, E., Limonta, M., Andò, S., Yang, S., 2016. Erosion patterns in the Changjiang (Yangtze River) catchment revealed by bulk–sample versus single–mineral provenance budgets. Geomorphology 261, 177–192. https://doi.org/10.1016/j.geomorph.2016.02.031.

Walling, D.E., Fang, D., 2003. Recent trends in the suspended sediment loads of the world's rivers. Glob. Planet. Chang. 39, 111–126. https://doi.org/10.1016/S0921–8181(03)00020–1.

Wan, S.M., Qin, L., Yang, S.Y., Zhao, D.B., Zhang, J., Jiao, D.F., Cai, G.Q., Pei, W.Q., Gong, H.M., Xu, Z.K., Huang, J., Yu, Z.J., Jin, H.L., Li, A.C., Li, T.G., 2020. South China Sea shelf weathering in glacial periods and its link to carbon cycle. Quater. Sci. 2020 (40), 1531–1549 (in Chinese with English abstract).

Wang, Z., Liu, J., Zhao, B., 2008. Holocene depocenter shift in the middle–lower Changjiang River basins and coastal area in response to sea level change. Front. Earth Sci. China 2, 17–26. https://doi.org/10.1007/s11707–008–0017–x.

Wang, L.C., Behling, H., Lee, T.Q., Li, H.C., Huh, C.A., Shiau, L.J., Chang, Y.P., 2014. Late Holocene environmental reconstructions and their implications on flood events, typhoon, and agricultural activities in NE Taiwan. Clim. Past 10, 1857–1869. https://doi.org/10.5194/cp–10–1857–2014.

Wei, X., Wu, C., 2011. Holocene delta evolution and sequence stratigraphy of the Pearl River Delta in South China. Sci. China Earth Sci. 54, 1523. https://doi.org/10.1029/2019GC008515.

Wessel, P., Luis, J.F., Uieda, L., Scharroo, R., Wobbe, F., Smith, W.H.F., Tian, D., 2019. The generic mapping tools version 6. Geochem. Geophys. Geosyst. 20, 5556–5564. https://doi.org/10.1029/2019GC008515.

Wu, G.Q., Liu, D.S., 1996. Land mollusk records from the Luochuan loess sequence and their paleoenvironmental significance. Sci. China (Series D) 26, 494–502.

Xu, K., Milliman, J.D., Li, A., Liu, J.P., Kao, S.J., Wan, S., 2009. Yangtze–and Taiwan–derived sediments on the inner shelf of East China Sea. Cont. Shelf Res. 29, 2240–2256. https://doi.org/10.1016/j.csr.2009.08.017.

Yang, Z.S., Liu, J.P., 2007. A unique Yellow River–derived distal subaqueous delta in the Yellow Sea. Mar. Geol. 240, 169–176. https://doi.org/10.1016/j.margeo.2007.02.008.

Yang, Z.S., Guo, Z., Wang, Z., Xu, J., Gao, W., 1992. The overall pattern of total suspended solids dispersal to the Yellow and East China Sea. Acta Oceanol. Sin. 14, 81–90 (in Chinese with English abstract).

Yang, T.F., Lee, T., Chen, C.H., Cheng, S.N., Knittel, U., Punongbayan, R.S., Rasdas, A.R., 1996. A double island arc between Taiwan and Luzon: consequence of ridge subduction. Tectonophysics 258, 85–101. https://doi.org/10.1016/0040–1951(95)00180–8.

Yang, T.N., Lee, T.Q., Meyers, P.A., Song, S.R., Kao, S.J., Löwemark, L., Shiau, L.J., 2011. Variations in monsoonal rainfall over the last 21 kyr inferred from sedimentary organic matter in Tung–Yuan Pond, southern Taiwan. Quat. Sci. Rev. 30, 3413–3422. https://doi.org/10.1016/j.quascirev.2011.08.017.

Yang, R.J., Liu, J.T., Fan, D., Burr, G.S., Lin, H.L., Chen, T.T., 2017. Land–sea duel in the late Quaternary at the mouth of a small river with high sediment yield. J. Asian Earth Sci. 143, 59–76. https://doi.org/10.1016/j.jseaes.2017.03.028.

Yao, T.D., 1997. A study on the climate changes from Guliya ice core records since last interglacial period. China Sci. (D) 6, 447–452.

Yin, H., Yu, G., 2000. Evolution of drainage systems and its developing trend in connection with tectonic uplift of Eastern Kunlun Mt. Chin. Sci. Bull. 45, 1904–1908.

Yokoyama, K., Tsutsumi, Y., Lee, C.S., Shen, J.J.S., Lan, C.Y., Zhao, L., 2007. Provenance study of tertiary sandstones from the Western foothills and Hsuehshan Range, Taiwan. Bull. Nat. Mus. Nat. Sci. Serial C 33, 7–26.

Zelilidis, A., 2000. Drainage evolution in a rifted basin, Corinth graben, Greece. Geomorphology 35, 69–85. https://doi.org/10.1016/S0169–555X(00)00023–4.

Zhang, X., Yan, Y., Huang, C.Y., Chen, D., Shan, Y., Lan, Q., Yu, M., 2014. Provenance analysis of the Miocene accretionary prism of the Hengchun Peninsula, southern Taiwan, and regional geological significance. J. Asian Earth Sci. 85, 26–39. https://doi.org/10.1016/j.jseaes.2014.01.021.

Zhang, X., Cawood, P.A., Huang, C.Y., Wang, Y., Yan, Y., Santosh, M., Yu, M., 2016. From convergent plate margin to arc–continent collision: Formation of the Kenting Mélange, Southern Taiwan. Gondwana Res. 38, 171–182. https://doi.org/10.1016/j.gr.2015.11.010.

Zhang, X., Huang, C., Wang, Y., Clift, P.D., Yan, Y., Fu, X., Chen, D., 2017. Evolving Yangtze River reconstructed by detrital zircon U-Pb dating and petrographic analysis of Miocene marginal Sea sedimentary rocks of the Western Foothills and Hengchun Peninsula, Taiwan. Tectonics 36, 634–651. https://doi.org/10.1002/2016TC004357.

Zhang, S., Jian, X., Pullen, A., Fu, L., Liang, H., Hong, D., Zhang, W., 2021. Tectono–magmatic events of the Qilian orogenic belt in northern Tibet: new insights from detrital zircon geochronology of river sands. Int. Geol. Rev. 63, 917–940. https://doi.org/10.1080/00206814.2020.1734876.

Zhao, Y., Yang, S., Liu, J.T., Fan, D., Yang, R.J., Bi, L., Chang, Y.P., 2017. Reconstruction of silicate weathering intensity and paleoenvironmental change during the late Quaternary in the Zhuoshui River catchment in Taiwan. Quat. Int. 452, 43–53. https://doi.org/10.1016/j.quaint.2016.12.013.